System Identification Using Discontinuous Data Sets

and PID Loop-shaping Control of A Vertical Take-off and Landing Drone

by

Yiqiu Liu

A Thesis Presented in Partial Fulfillment
of the Requirements for the Degree
Master of Science

Approved October 2015 by the
Graduate Supervisory Committee:

Konstantinos S. Tsakalis, Co-Chair
Armando A. Rodriguez, Co-Chair
Daniel E. Rivera

ARIZONA STATE UNIVERSITY

December 2015

ABSTRACT

Vertical taking off and landing (VTOL) drones started to emerge at the beginning of this century, and finds applications in the vast areas of mapping, rescuing, logistics, etc. Usually a VTOL drone control system design starts from a first principles model. Most of the VTOL drones are in the shape of a quad-rotor which is convenient for dynamic analysis.

In this project, a VTOL drone with shape similar to a Convair XFY-1 is studied and the primary focus is developing and examining an alternative method to identify a system model from the input and output data, with which it is possible to estimate system parameters and compute model uncertainties on discontinuous data sets. We verify the models by designing controllers that stabilize the yaw, pitch, and roll angles for the VTOL drone in the hovering state.

This project comprises of three stages: an open-loop identification to identify the yaw and pitch dynamics, an intermediate closed-loop identification to identify the roll action dynamic and a closed-loop identification to refine the identification of yaw and pitch action. In open and closed loop identifications, the reference signals sent to the servos were recorded as inputs to the system and the angles and angular velocities in yaw and pitch directions read by inertial measurement unit were recorded as outputs of the system. In the intermediate closed loop identification, the difference between the reference signals sent to the motors on the contra-rotators was recorded as input and the roll angular velocity is recorded as output. Next, regressors were formed by using a coprime factor structure and then parameters of the system were estimated using the least square method. Multiplicative and divisive uncertainties were calculated from the data set and were used to guide PID loop-shaping controller design.

ACKNOWLEDGMENTS

I would like to sincerely thank several people who have advised, assisted, encouraged or inspired me finishing this thesis.

First, I would like to express my deepest gratitude to my adviser Dr. Konstantinos Tsakalis. I took his Computer Controlled System, Nonlinear System Theory, Adaptive Control and Optimal Control courses and I learned a lot from his lectures which helped me understand the fundamentals of control system. He also provided me with this fantastic opportunity to work on this project and kindly offer me guidance on experiment design and data processing. His dedication to academics impacted me deeply and I feel honored to have been under his mentorship.

Secondly I would like to thank Prof. Armando Rodriguez and Prof. Daniel Rivera. I took Prof. Rodriguez's Linear System Theory course and Prof. Rivera's Introduction to System Identification course. Both of these courses are closely related to my thesis.

I would to thank Mr.Coby Leuschke and Prof. Thomas Taylor. Without them, I would never had the chance to participate this project. Mr. Leuschke donated the drone to us for this project and Prof. Taylor kindly introduced Mr. Leuschke to us, and Prof. Taylor also provided precious advises on the experiment design and data processing.

I would also like to thank my labmates, Md Shafique, Rakesh Joshi, Victoria Rodriguez, and Garret Scott. Without their help I would never have been able to conduct my experiments. Special thanks to Shafique for his guidance and encouragement in my research. His optimism and patience impacted me greatly and I feel lucky to have the chance to work with him.

And I would like to thank Justin Echols, for his help to my homework of APM503 in this Fall 2015 semester, as well as finding typos in this thesis.

Great appreciation to my parents who have supported me with my academic study. Without their effort, I would never have the chance of pursuing a Master of Science degree.

Last but not least, I want to say thank you to my better half, Yifan Zhao, for her endless love, patience and support during my research.

TABLE OF CONTENTS

CHAPTER Page

LIST OF FIGURES

Chapter 1

INTRODUCTION

1.1 Overview

VTOL drones have gained great popularity since the beginning of this century. They have been widely used in surveillance, mapping, and rescuing. Recently, Amazon.com has been experimenting with delivering packages via VTOL drones.

The advantages of VTOL drones include their ability to take off and land almost everywhere as well as its ability of switching between hovering mode and forward flying mode. They are usually small in size such that they could be dispatched to situations that have limited room for the task. Also due to recent development in power electronics and electric machines, VTOL drones now have higher capability of carrying weights.

Unfortunately, VTOL drone also comes with the disadvantage of being vulnerable as it is easily affected by wind. Thus, it is critical for the control system to reject the disturbances from wind and other factors and stabilize the drone. Another issue with VTOL drones is the navigation, for the consideration of cost-performance, the inertia measurement units (IMU) on VTOL drones do not have high precisions. This is also due to the limitation of its size as high precision IMU modules are often heavy and big in size. Thus it's a challenge to design control and navigation systems for VTOL drones to provide enough guarantee for the fulfillment of their tasks.

The design of navigation system precedes the control system as the control system, typically referred as feedback control system, will have to take in the position and attitude information provided by the navigation system as input. The position

and attitude information is acquired from attitude estimation and position estimation. Attitude estimation makes use of an IMU which typically comprises of an accelerometer and a gyroscope that collect acceleration and Euler angular rates. Depending on the algorithm used for attitude estimation, sometimes a magnetometer will be used for collecting Euler angles. Attitude estimation also makes use of acceleration data to complement the gyroscope and magnetometer data. Position estimation uses a GPS receiver and a barometer that collects the coordinate and height, as well as the acceleration data from IMU. For the present stage of this project, the focus is on maintaining the hovering status, position estimation is not the main purpose of using the acceleration data.

A well designed control system is necessary for a VTOL drone to fly as users would demand. Generally speaking, the features of a control system we need to take into considerations are: the transient response (including settle time, overshoot and undershoot), the steady state error, the sensitivity to the disturbance, and the easiness for implementation. For a VTOL drone, the transient response is the most important thing as taking off could be vital, especially in the presence of wind it needs to take off fast and settle quickly. In the hovering status, steady state error will cause the drone to drift, so the system should minimize steady state error. With the disturbance from the wind, vibration from the motors, measurement noises and quantization error from digital implementation, the system will have certain level of uncertainties. The robustness performance is the ability of the VTOL drone to remain steady in the presence of uncertainties and is one of the targets for controller design in this project. While good system performance could be achieved by using advanced and complex control algorithms, we still need to consider the ease of implementation. Usually, the performance of a computational source is positive related to the size and weight of it.

With limited weight carrying capability, we need to use simple yet high performance controller such as PID algorithm for an embedded system implementation.

In a systematic way of controller design, it is necessary to acquire a model either in form of transfer function or differential equations. System identification is to estimate system parameters from input and output data sets. For this project, linear time invariant systems at the equilibrium of hovering state were identified. By designing controllers for the models, the VTOL drone will stay hovering in the air, the pitch and yaw angles will be in the vicinity of zero.

Traditionally, for the input signals, leading zeros and ending zeros should be added to guarantee the system starts from rest and ends in rest. However, in the system identification experiments of the VTOL drone, especially in the open loop test, there was no controller that regulates the attitude of the drone and the drone would quickly crash into the ground or hit the tethers which were used for restricting the movement of the drone. Thus the input and output data have to be truncated in which the VTOL drone is not hitting anything and the Euler angles are not too deviated from zero. In this case, the data sets will be short and discontinuous which are not suitable for traditional identification methods. An innovative way of constructing estimation problems in system identification is proposed in this thesis that can make use of these discontinuous data sets to get reliable models.

1.2 Literature Review

For the purpose of maintaining the hovering status, attitude estimation is the primary focus in the navigation system because as long as the yaw and pitch angles are zero, the VTOL drone would not fall down. When processing attitude data, it should be noticed that the data from magnetometers are usually with respect to the earth

gravity frame while the accelerometer and gyro-meter data are usually with respect to the VTOL drone body frame. As the controller will be designed with respect to the earth frame as input, the next step is sensor fusion in which the acceleration, angular rate, and Euler angles will be all be corrected and converted to the earth frame. Various methods have been developed to take care of this step such as Kalman filter based sensor fusion as presented in [22] and [5], Madgwick's quaternion based gradient descent algorithm as presented in [20] and [19], and Mahony's nonlinear complementary filter as presented in [21] and [14]. Madgwick's and Mahony's algorithms are realized in FreeIMU which is an open source project that provides both hardware realization to build navigation system as well as a software library that read and process the data from IMU as represented in [37] [38].

If a system is fully known, the system model can be built from first principles. McRuer *et al* elaborate the modeling and control of aircraft from aerodynamics in [24]. And [3] written by Bouabdallah *et al* is a tutorial to the modeling and control of an indoor purposed quadrotor, which is the most popular kind of VTOL drone. Although first principles can provide sufficiently accurate models, there are always unknown parameters to be determined in a system numerically. System identification is another way of building models for a physical system. System identification could be classified by how much we known about the system. Black box system identification is suitable for cases where the system is completely unknown and gray box identification is suitable for cases where the system parameters are partially known [29]. Another necessity in system identification is that parameters could be varying, such as for controlling time varying systems, we have to carry out system identification online to determine the parameters of the controller for the purpose of indirect adaptive control [32].

System identification is the application of parameter estimation in control community. The key is to provide persistent excitation to the system and collect the output as shown in [27] by Saaverdra *et al.* The excitation could be in form of step signal, sum of sinusoid signals, random binary sequence (RBS) and pseudo-random binary sequence (PRBS) with enough bandwidth. To process the input and output (I/O) data set and identify the system, the mainstream methods are the subspace identification method (SIM) and the prediction error methods (PEM) [11]. The subspace identification utilizes projection and provides state space representation for the model. The only parameter for users to select is the order of the model. In addition, SIM features the fast convergence rate and numerical stability [36]. Model reduction is also necessary to achieve an appropriate order of the system [26]. PEM utilizes many structures of models to describe the system and the disturbance, such as auto-regressive–moving-average model with exogenous inputs (ARMAX) model as presented by Ding *et al* in [7], Box-Jenkins model as presented by Ding *et al* in [6] and Output-Error model as presented by Ding *et al* in [8] Prediction error method tries to identify a system parameter vector that minimizes the prediction error and makes the residue uncorrelated to the system input [17]. PEM has the advantage of the ability to be easily applied in closed loop control. This method is closely related to the maximum likelihood estimation and thus has good asymptotic property [18]. Drawbacks of the traditional SIM and PEM are their lack of description of the uncertainties in the system: they assumed that the input and disturbances are uncorrelated, which is only an ideal condition [26]. The controller designed might stabilize the identified plant, however, as the uncertainties are not systematically considered in the design, there is no guarantee for the robust stability.

With the development of robust control theory, the emerging field of identification for control helps alleviate this problem. Tsakalis and Zhan presented two

robust-control-oriented system identification methods in [41] and [42]. The introduction of an iterative identification method using normalized coprime factor structure in [35] presents a necessary and sufficient condition for the guarantee of the robust stability in the controller design. Similar conclusions can also be achieved by applying small gain theorem [43]. On the computation aspect of the coprime factor uncertainty estimation, it is normally an optimization problem for the fitting error and can be viewed as the sum of the perturbation from both input and output, which is an one equation two unknowns problem. The problem could be solved by applying the gap metric computation introduced in [10]. However, several sub-optimal solutions that are simple to implement could be achieved by applying the method introduced in [33], [31] and [34]. These methods are based on the assumption that the error contribution from the input and that from output are orthogonal, and compute the uncertainty bounds at frequency of interest (around bandwidth of the system). Target loop complementary sensitivity and sensitivity bounds should be carefully selected and provided for these methods, which means the optimization depends on the actual controller. A comparison has been made between the coprime factor uncertainty estimation and other methods in [1], which carried out a paper machine case study. In the case study, it showed that coprime factor method has the advantages of accurately predicting the stability bounds and low demand on computational resources.

Various control design methods could be modified to be able to achieve a controller that stabilizes the system, rejects the disturbance, while satisfies the robust stability conditions (RSC). For example in [15], by applying linear matrix inequality (LMI) method to solve a problem of minimizing an upper bound on the worst case function, it is possible to formulate the model predictive control problem with description of uncertainties. In [13], it is possible to select a target loop that satisfies

the RSC and then solve a convex optimization problem to get PID controller coefficients that is closest to the loop shape. It is also possible to get an discrete-time PID controller directly using the loop shaping methods as shown in [28] by Shafique and Tsakalis, which is convenient for control implementation on computers. However, it should be noticed that there is a trade-off between maximizing the performance and the guaranteeing robustness. A general method to get an optimal balance between performance and robustness using H_{inf} optimization for multiple input and multiple out case is proposed in [23].

1.3 Thesis Organization

This thesis is organized in six chapters.

In chapter 2, methods and techniques used in the system identification of this project is presented: least square methods, coprime factorization of a system and the uncertainty computation methods used in this project.

Chapter 3 contains the controller design methods including LQR, H_{inf} control and the loop shaping method to acquire the PID parameters.

In chapter 4, we discuss the VTOL drone studied in this project and the system identification experiment, including implementation of controllers designed for the identified systems.

In chapter 5, the results of the experiments and the controllers designed for each stages were presented.

In chapter 6, the conclusion, discussion, and the future work for this project were presented.

Chapter 2

SYSTEM IDENTIFICATION METHODS USING MULTIPLE DISCONTINUOUS DATA SETS

2.1 Introduction

In this chapter, the method used for identifying a system model from discontinuous data sets is presented. The discussion begins by formulation of the estimation problem, which takes the initial condition of the system into consideration. Follows by the identifying MIMO systems by partitioning them into MISO systems. Next, the way to construct estimation problems on multiple data sets is presented. A brief introduction of the least square method used for solving the estimation problem is also presented.

Robust stability is one of the major consideration in the control system design, which requires the uncertainties in the identification results to be provided. And in the second half of this chapter, the computation of the estimation error, co-prime factor uncertainties, multiplicative uncertainty and divisive uncertainty in the system is elaborated. The usage of multiple and discontinuous data sets in the computation is introduced at the end of this chapter.

2.2 Estimation Problem Formulation for Discontinuous Data Sets

First we take a look at tradition way of coprime factorization on transfer function described system. For the case of a MISO system $\mathbf{P} : u \in \mathbf{R}^n \mapsto y \in \mathbf{R}^1$, we have the

transfer function matrix as the following:

$$\mathbf{P}(s) = \left[\frac{N_1(s)}{D_1(s)} \cdots \frac{N_i(s)}{D(s)} \cdots \frac{N_n(s)}{D(s)} \right] \tag{2.1}$$

For a single element $P_i(s) = \frac{N_i(s)}{D(s)}$, we have the following:

$$P_i(s) = \frac{N_i(s)}{D(s)} = \frac{N_{i,1}s^{n_i} + N_{i,2}s^{n_i-1} + \cdots + N_{i,n+1},}{s^m + D_1 s^{m-1} + \cdots + D_m} \tag{2.2}$$

And we can write the input and output as

$$y_i(t) = \frac{N_i(s)}{D(s)}[u_i(t)] \tag{2.3}$$

Where $y(t) = \sum y_i(t)$. For a proper transfer function, we always have $m > n_i$. It is necessary to have an auxiliary filter $\frac{1}{F(s)} = \frac{1}{s^m + F_1 s^{m-1} + \cdots + F_m}$ for the coprime factorization:

$$y_i(t) = \frac{N_i(s)}{F(s)}[u_i(t)] + \frac{F(s) - D(s)}{F(s)}[y_i(t)] = W^\top \theta_i$$

Where

$$W = \left[\frac{s^{n_i}}{F(s)}[u_1(t)] \cdots \frac{1}{F(s)}[u_n(t)] \ , \frac{s^{m-1}}{F(s)}[y_i(t)] \cdots \frac{1}{F(s)}[y_i(t)] \right]^\top \tag{2.4}$$

and

$$\theta_i = \begin{bmatrix} N_{i,1} \\ \vdots \\ N_{i,n+1} \\ F_1 - D_1 \\ \vdots \\ F_m - D_m \end{bmatrix} \tag{2.5}$$

For MIMO system identification case, it is convenient to identify by decomposing the MIMO system to a bunch of MISO systems and combine them together to form the final system. The auxiliary filter $F(s)$ should be selected such that the bandwidth

is greater or equal to the bandwidth of the target system but less than the Nyquest frequency, and the order should be the same with the target system. In this sense, it is a grey-box identification process, in which some a-prior information of the system should be acquired.

An issue with this formulation is that the initial condition is not taken into consideration. For discontinuous data sets, at the beginning of each data set, the system is not necessarily at rest, for systems with unstable modes, this will cause huge error. To solve this, we can make the initial conditions being part of the parameters to be estimated. Using a state-space formulation is convenient for integrating the estimation of initial conditions. We as well first consider a MISO system case. For a system $G(A, B, C, D) : u(t) \in \mathbf{R}^n \mapsto y(t) \in \mathbf{R}$ with order p, we can write the differential equations as:

$$\dot{x} = Ax + bu,\ y = Cx + Du \tag{2.6}$$

We can select a matrix L such that $F = A - LC$ is Hurwitz and write they system as

$$\dot{x} = Ax + Bu + Ly - Ly,\ y = Cx + Du \tag{2.7}$$

The pre-selected pair (F, q) should be completely observable and F should be Hurwitz. A good way to choose (F, q) is to first choose the auxiliary filter $F(s)$, and then convert it to balanced realized state-space representation and (F, q) is the (A, C) matrix of the state-space representation. Equation 2.7 could be written as

$$\dot{x} = Fx + \theta_1 u + \theta_2 y,\ y = qx + \theta_3 u \tag{2.8}$$

where $F = A - LC$, $\theta_1 = B - LD$, $\theta_2 = L$, $q = C$, $\theta_3 = D$. And solution to the above equations is

$$y = q(sI - F)^{-1}\theta_1 u + q(sI - F)^{-1}\theta_2 y + \theta_3 u + q(sI - F)^{-1}x_0 \tag{2.9}$$

Since this is the MISO system, the above could be written as

$$y = \sum_{i=1}^{n} q(sI - F)^{-1} u_i \theta_{1i} + q(sI - F)^{-1} \theta_2 y + \sum_{i=1}^{n} u_i \theta_{3i} + q(sI - F)^{-1} x_0 \qquad (2.10)$$

where θ_{1i} is the column of θ_1, u_i is the element of u, and θ_{3i} are rows of θ_3. equation 2.10 could be written as:

$$y(t) = w^\top \theta \qquad (2.11)$$

where

$$\begin{aligned} w = [&q(sI - F)^{-1}[u_1(t)] \cdots q(sI - F)^{-1}[u_n(t)] \cdots \\ &q(sI - F)^{-1}[y(t)] \;\; u_1(t) \cdots u_n(t) \; q(sI - F)^{-1}]^\top \end{aligned} \qquad (2.12)$$

and

$$\theta = \left[\theta_{11}^\top \ldots \theta_{1n}^\top \; \theta_2 \; \theta_{31}^\top \ldots \theta_{3n}^\top \; x_0^\top \right]^\top \qquad (2.13)$$

Here the initial condition is considered as parameters that could be estimated together with system parameters from discontinuous data. In MATLAB, functions lsim() and expm() could be used to construct the regressors.

2.3 MIMO Case and Multiple Data Sets

The above formulation is suitable for MISO systems. Consider a MIMO system in state space representation $G_{[A,B,C,D]} : u(t) \in \mathbf{R}^n \mapsto y(t) \in \mathbf{R}^m$. In this case, we can convert the identification of a MIMO system to combination of the identification of each MISO system in it. First we partition the system as shown in equation 2.14 and G_i takes all input and generates the ith output.

$$\begin{aligned} G &= \left[G_1 \cdots G_i \cdots G_n \right]^\top \\ G_i &: u(t) \in \mathbf{R}^n \mapsto y_i(t) \in \mathbf{R} \end{aligned} \qquad (2.14)$$

Model order reduction is a recommended step with which a minimal system will be acquired.

For multiple data sets, it is necessary to concatenate the regressors constructed on each date sets. Suppose data sets $(u_1, y_1), \cdots, (u_k, y_k)$ are input and output data sets collected in the system identification experiments on a MIMO system $G_{[A,B,C,D]}$: $u(t) \in \mathbf{R}^n \mapsto y(t) \in \mathbf{R}^m$ with pth order. To identify this system MIMO system, we first partition the system as in equation 2.14. Then we partition each data set (u_i, y_i) as $(u_i, y_i1), \ldots, (u_i, y_im)$. And the regressor for G_j is constructed as $\omega_j = \left[\omega_{1j}^\top \ldots \omega_{kj}^\top\right]^\top$ where ω_{ij} is

$$\begin{aligned}\omega_{ij} = \big[&q(sI-F)^{-1}[u_{i1}(t)] \ldots q(sI-F)^{-1}[u_{in}(t)]\ q(sI-F)^{-1}[y_{ij}(t)] \ldots \\ &u_{i1}(t) \ldots u_{in}(t)\ O_{1j}\ q(sI-F)^{-1}\ O_{2j}\big]^\top\end{aligned} \tag{2.15}$$

And O_{1j} is a zero matrix with $p(i-1)$ columns and O_{2j} is a zero matrix with $p(k-i)$ columns. The parameter vector θ_j for G_j is

$$\theta_j = \left[\theta_{11,j}^\top \ldots \theta_{1n,j}^\top\ \theta_{2,j}^\top\ \theta_{31,j}^\top \ldots \theta_{3n,j}^\top\ x_{0,j1}^\top \ldots\ x_{0,jk}^\top\right]^\top \tag{2.16}$$

where $x_{0,ji}$ is the initial condition of G_j in the ith data set. Then construct vector Y_j as

$$Y = \left[y_{1j}^\top \ldots y_{kj}^\top\right]^\top \tag{2.17}$$

Thus the system parameter problem could be formulated as

$$Y_j = \omega_j^\top \theta_j \tag{2.18}$$

By solving equation2.18, the system parameters of G_j is acquired. Next, as before, the MIMO system G is acquired by concatenating each G_j estimated and carrying out an order reduction procedure to get a minimal system.

2.4 Least Square Estimation Methods

For solving the estimation problem, there are various estimation methods: best linear unbiased estimation (BLUE) as presented in [16] by Legarra *et al*, maximum likelihood estimation as presented in [39] by Wang *et al*. These methods require that the probability distribution function known a priori. However, as the Gaussian distribution is the best guess, and thus we use least square estimation to solve equation 2.11 and 2.18.

For system identification on data set gathered from experiments, it is suitable for a batch processing. For example, to solve equation 2.18, we formulate the optimization problem as

$$\min_{\theta_j} \| Y_j - \omega_j^\top \theta \|_2 \tag{2.19}$$

Solution to the above is

$$\hat{\theta_j} = (\omega_j \omega_j^\top)^{-1} \omega_j Y_j \tag{2.20}$$

2.5 Estimation Error Computation

Estimation error is the difference between the output achieved by the minimizer of equation 2.11 and the real output: $e(t) = y(t) - \hat{y}(t)$. Where

$$\hat{y}(t) = q(sI - F)^{-1}\hat{\theta}_1 u + q(sI - F)^{-1}\hat{\theta}_2 y + \hat{\theta}_3 u + q(sI - F)^{-1}\hat{x}_0 \tag{2.21}$$

However, there exist conditions where it is required to compute the uncertainties of a given system on a given data set (u_v, y_v). For the consideration that the system may not be at rest at the start, the first thing needed is to estimate the initial condition of

the coprime factorized system. By choosing $F(s)$ and computing (F, q) pair described in section 2.2, we will have the following:

$$y_v(t) = w_u\theta_u + w_y\theta_y + w_{x_0}x_0 \tag{2.22}$$

where

$$w_u = \left[q(sI - F)^{-1}[u_{v1}(t)] \cdots q(sI - F)^{-1}[u_{vn}(t)],\ u_{v1}(t) \cdots u_{vn}(t)\right]$$

$$w_y = q(sI - F)^{-1}[y_v(t)]$$

$$w_{x_0} = q(sI - F)^{-1}$$

$$\hat{\theta}_u = \left[\hat{\theta}_1\ \hat{\theta}_3\right]$$

$$\hat{\theta}_y = \hat{\theta}_2$$

The initial condition could be estimated by solving the following optimization problem.

$$\begin{aligned} \min_{x_0} \quad & \parallel e_v(t) \parallel_2 \\ \text{s.t.} \quad & e_v(t) = y_v(t) - (w_u\hat{\theta}_u + w_y\hat{\theta}_y + w_{x_0}x_0) \end{aligned} \tag{2.23}$$

and $e_v^*(t)$achieved by the optimizer x_0^* could be used for the uncertainty computation.

2.6 Coprime Factor Uncertainty Computation

The system with coprime factor uncertainties are shown in Figure 1. Δ_N is the uncertainty on the numerator and Δ_D is the uncertainty on the denominator. For the nominal system $G = NM^{-1}$, the actual system will be

$$y(t) = (N_F + \Delta_N)(D_F + \Delta_D)^{-1} \tag{2.24}$$

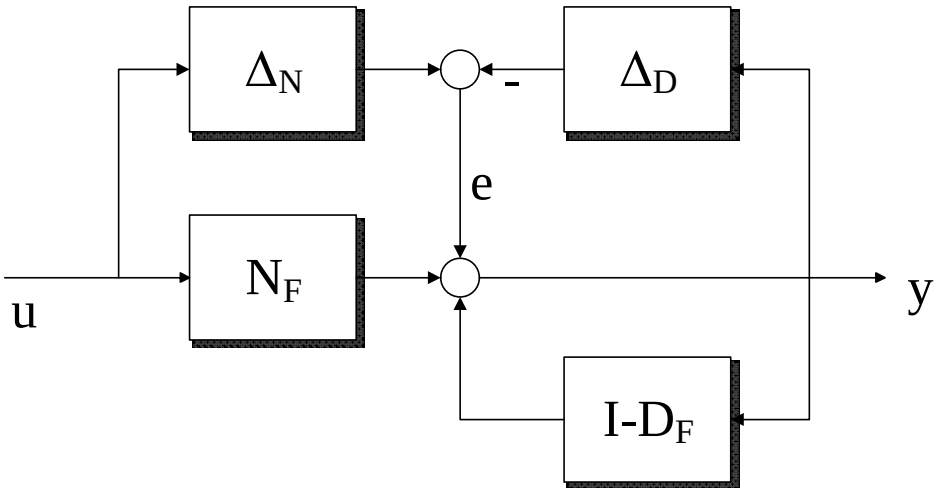

Figure 1. Coprime factor uncertainty structure

From the coprime factor structure shown in Figure 1, the estimation error is the contribution of both the input ant output:

$$e(t) = \Delta_N[u(t)] + \Delta_D[y(t)] \tag{2.25}$$

In [33], an unfalsification approach of computing Δ_D and Δ_N is introduced, which seeks the most favorable bounds for Δ_D and Δ_N that describes the estimation error. Here a brief description of this method is presented for the consideration of a square system. By applying the small gain theorem, we get the robust stability condition for system with coprime factorization structure:

$$\bar{\sigma}[P^{-1}TD_F^{-1}]\bar{\sigma}[\Delta_N] + \bar{\sigma}[SD_F^{-1}]\bar{\sigma}[\Delta_D] < 1 \tag{2.26}$$

The coprime factor uncertainty computation is then converted to the following optimization problem:

$$\begin{aligned} \min_{\delta_1,\delta_2} \quad & \bar{\sigma}[P^{-1}TD_F^{-1}]\delta_1 + \bar{\sigma}[SD_F^{-1}]\delta_2 < 1 \\ \text{s.t.} \quad & \Delta_N[u] + \Delta_D[y] = e \\ & \bar{\sigma}[\Delta_N] \le \delta_1, \bar{\sigma}[\Delta_D] \le \delta_2 \end{aligned} \tag{2.27}$$

By selecting a target loop complementary sensitivity function $T(s)$ and sensitivity function $S(s)$, the method in [33] provides a sub-optimal solution to Δ_N and Δ_D under the assumption $\Delta_N[u] \perp \Delta_D[y]$:

$$\delta_1 = \frac{\Phi_e(\omega)}{\Phi_u(\omega)} \frac{1}{\sqrt{1+l^2}};\ \delta_1 = \frac{\Phi_e(\omega)}{\Phi_y(\omega)} \frac{l}{\sqrt{1+l^2}} \tag{2.28}$$

where

$$l = \frac{\Phi_y(\omega)}{\Phi_u(\omega)} \frac{\bar{\sigma}[P^{-1}]\bar{\sigma}[T]}{\hat{\sigma}[S]} \tag{2.29}$$

For the coprime factor uncertainties computed using this method, the robust stability condition is achieved if the targeted complementary sensitivity and sensitivity functions are higher than or equal to those achieved by the controller. In equation 2.28, $\Phi_e(\omega)$, $\Phi_u(\omega)$ and $\Phi_y(\omega)$ could be calculated through the algorithm introduced in [40].

For multiple data sets $(u_1, y_1), \cdots, (u_i, y_i), \cdots, (u_n, y_n)$, estimation error $e_1, \cdots, e_i, \cdots, e_n$ could be computed from each data sets using equation 2.21 or 2.23, and power spectrum $(\Phi_{e_1}\Phi_{u_1}, \Phi_{y_1}), \cdots, (\Phi_{e_i}, \Phi_{u_i}, \Phi_{y_i}), \cdots, (\Phi_{e_n}\Phi_{u_n}, \Phi_{y_n})$ could be computed on each data sets through algorithms introduced in [40] respectively. To compute the uncertainties, the mean square of these are taken:

$$\begin{aligned}
\Phi_e(\omega_i) &= \sqrt{\frac{1}{n}\sum_{j=1}^{n} \Phi_{e_j}^2(\omega_i)} \\
\Phi_u(\omega_i) &= \sqrt{\frac{1}{n}\sum_{j=1}^{n} \Phi_{u_j}^2(\omega_i)} \\
\Phi_y(\omega_i) &= \sqrt{\frac{1}{n}\sum_{j=1}^{n} \Phi_{y_j}^2(\omega_i)}
\end{aligned} \tag{2.30}$$

2.7 Multiplicative and Divisive Uncertainty

The robust stability conditions for multiplicative Δ_M and divisive Δ_F structured uncertainties are

$$\begin{aligned} \| T(j\omega)\Delta_M(\omega) \|_\infty < 1 \\ \| S(j\omega)\Delta_F(\omega) \|_\infty < 1 \end{aligned} \tag{2.31}$$

Here we assume that the multiplicative uncertainty structure is adequate for representing the uncertainty bounds by itself and the same with the divisive uncertainty. In this condition, the multiplicative uncertainty is contributed by perturbations from the input signal and the divisive uncertainties is contributed by perturbations from the output. Then we would have:

$$\begin{aligned} \Delta_M = \frac{\Phi_e(\omega)}{\Phi_u(\omega)} \times \frac{1}{\underline{\sigma}[N_F]} \\ \Delta_F = \frac{\Phi_e(\omega)}{\Phi_y(\omega)} \times \frac{1}{\underline{\sigma}[D_F]} \end{aligned} \tag{2.32}$$

An alternative approach is based on the argument $\Delta_N[u] \perp \Delta_D[y]$. This assumption along with the fact that the complementary sensitivity function contributes more to the low frequency range while the sensitivity function contributes more to the high frequency range enable us to convert the coprime factor uncertainties to multiplicative and divisive uncertainties structure.

$$\begin{aligned} \Delta_M = \frac{\Delta_N}{\underline{\sigma}[N_F]} \\ \Delta_F = \frac{\Delta_D}{\underline{\sigma}[D_F]} \end{aligned} \tag{2.33}$$

If the robust stability condition 2.26 for coprime factor structure is achieved, with the assumption $\Delta_N[u] \perp \Delta_D[y]$, 2.31 is guaranteed. In addition, for MIMO systems, we distinguish between the multiplicative uncertainty at input and the multiplicative

uncertainty at output. If equation 2.33 is adopted, we will have

$$\begin{aligned} N_F(\Delta_{M_{in}} + I) &= N_F + \Delta_N \\ \Rightarrow \Delta_{M_{in}} &= N_F^{-1}\Delta_N \end{aligned} \tag{2.34}$$

and

$$\begin{aligned} D_F^{-1}(\Delta_N + N_F) &= (I + \Delta_{M_{out}})D_F^{-1}N_F \\ \Rightarrow \Delta_{M_{out}} &= D_F^{-1}\Delta_N P^{-1} \end{aligned} \tag{2.35}$$

Chapter 3

PID LOOP SHAPING CONTROLLER

3.1 Introduction

In this chapter we focus on the controller design part. The methods used for controller design are from [13] and [31]. The chapter begins by the introduction of concepts of the infinity norm of signals and systems. Then H_∞ controller design algorithms is presented and we also demonstrate the Linear Quadratic Regulator (LQR) design algorithms. Next, the loop shaping algorithms which searches for the optimized PID controller that shapes the loop as close as possible to the selected target loop is elaborated.

3.2 Infinity Norms of Signals and Systems

Here we distinguish between the infinity norms of signals and systems. For a signal $s(t)$, its infinity norm is:

$$\| s(t) \|_\infty = \sup_t |s(t)| \tag{3.1}$$

And for a system $P : u(t) \mapsto y(t)$, its infinity norm is:

$$\| P \|_\infty = \sup_{\| u \|_\infty \neq 0} \left(\frac{\| y(t) \|_\infty}{\| u(t) \|_\infty} \right) \tag{3.2}$$

3.3 H_∞ Controller Design

The H_∞ design guarantees the robustness of the system in the sense of H_∞ as it minimizes the H_∞ norm of the loop. For standard H_∞ controllers, depending on the user's selection, the complementary sensitivity function or the sensitivity function is designed to be placed below the bounds indicated by corresponding uncertainties computed from the system identification experimental data sets. [30] gives detailed derivation for the design of H_∞ controller, the procedure is briefly introduced in this section.

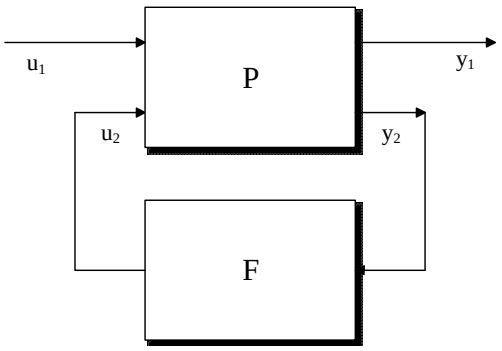

Figure 2. Standard H_∞ control connection scheme

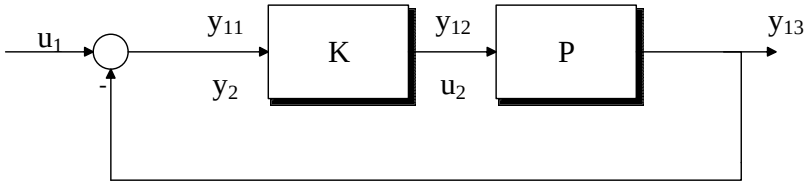

Figure 3. Transformation of control loop to H_∞ standard control connection scheme

For a system control loop in 3, it is possible to transform it to the form of Figure 2, the inputs to the system are u_1, which is the reference signal, and u_2 which is

the manipulated signal. The outputs of the system are y_1, the error signal and the measured output y_2. The relation between (u_1, u_2) and (y_1, y_2) are:

$$\begin{bmatrix} y_1(t) \\ y_2(t) \end{bmatrix} = \begin{bmatrix} P_{11}(s) \; P_{12}(s) \\ P_{21}(s) \; P_{22}(s) \end{bmatrix} \left[\begin{bmatrix} u_1(t) \\ u_2(t) \end{bmatrix} \right] \tag{3.3}$$

Now we can partition the system as

$$P = \begin{bmatrix} A \; B \\ C \; D \end{bmatrix} = \begin{bmatrix} A \; B_1 \; B_2 \\ C_1 \; D_{11} \; D_{12} \\ C_2 \; D_{12} \; D_{22} \end{bmatrix} \tag{3.4}$$

which means

$$\begin{aligned} \dot{x} &= Ax + B_1 u_1 + B_2 u_2 \\ y_1 &= C_1 x + D_{11} u_1 + D_{12} u_2 \\ y_2 &= C_2 x + D_{12} u_1 + D_{22} u_2 \end{aligned} \tag{3.5}$$

In H_∞ design procedure, the target is to find a controller K such that with $K : y_2 \mapsto u_2$, the system $T : u_1 \mapsto y_1$ is stable and has small H_∞ norm. When the system is LTI, we can write T as:

$$T(s) = P_{11}(s) + P_{12}(s) \left[I - K(s) P_{22}(s) \right]^{-1} K(s) P_{21}(s) \tag{3.6}$$

The formulation of the problem could be either in the form of minimizing the H_∞ norm (optimal H_∞ control) or making the H_∞ norm under a certain level (standard H_∞ control). Generally we have:

$$\begin{aligned} \min_{K} \quad & \| \, T_{u_1, y_1} \, \|_\infty \\ \text{s.t.} \quad & \| \, T_{u_1, y_1} \, \|_\infty < \gamma \end{aligned} \tag{3.7}$$

For a special case where the internal stability is guaranteed and the system is both stabilizable and observable, we can write down the minimal entropy controller which is also called the central controller:

$$K_\infty = \begin{bmatrix} A_\infty & -Z_\infty L_\infty \\ F_\infty & 0 \end{bmatrix} \tag{3.8}$$

where

$$\begin{aligned} A_\infty &= A + \gamma^{-2} B_1 B_1^\top X + B_2 F_\infty + Z_\infty L_\infty C_2 \\ F_\infty &= -B_2^\top X \\ L_\infty &= -Y C_2^\top \\ Z_\infty &= \left(I - \gamma^{-2} Y X\right)^{-1} \end{aligned} \tag{3.9}$$

where $X \geq 0$, and is the solution to the control Riccati equation

$$A^\top X + XA + X\left(\gamma^{-2} B_1 B_1^\top - B_2 B_2^\top\right) X + C_1^\top C_1 = 0 \tag{3.10}$$

and $Y \geq 0$, which is the solution to the observer Ricatti equation

$$YA^\top + AY + Y\left(\gamma^{-2} C_1 C_1^\top - C_2 C_2^\top\right) X + B_1 B_1^\top = 0 \tag{3.11}$$

3.4 Linear Quadratic Regulator

Linear quadratic regulators minimize a cost function in the quadratic forms by generating specific control input. For a system in form of of 2.6, the object function is selected as:

$$J = \int_0^\infty \left[x^\top(t) Q x(t) + u^\top T(t) R u(t)\right] dt \tag{3.12}$$

by applying algorithms introduced in [25], we can have the control input to the system as

$$u = Kx = -R^{-1}B^{\top}Px \tag{3.13}$$

where P is the solution to the control Riccati equation

$$A^{\top}P + PA - PBR^{-1}B^{\top}P + Q = 0 \tag{3.14}$$

The system is guaranteed to be asymptotically stable as long as Q and R are positive definite.

3.5 PID Tuning by Frequency Loop Shaping

Proportional-Integral-Derivative (PID) controller is a feedback control implementation with a proportional filter, a integral filter, and a derivative filter, and is widely used in industry. Although there are all kinds of control design algorithms, a simple and reliable way introduced in [12] is to use frequency loop shaping optimization to get an PID controller C for the plant G that makes the loop GC close to the targeted loop L we designed using algorithms like H_∞ and LQR as described in previous sections in the sense of H_∞ norm. A PID control law is:

$$u(t) = C(s)[r(t) - y(t)] = \left[K_p + \frac{K_i}{s} + \frac{K_d s}{\tau s + 1}\right][r(t) - y(t)] \tag{3.15}$$

The $C(s)$ is equivalent to

$$C(s) = \frac{K_1 s^2 + K_2 s + K_3}{s(\tau s + 1)} \tag{3.16}$$

where

$$\begin{aligned} K_p &= K_2 - K_3\tau \\ K_i &= K_3 \\ K_d &= K_1 - K_2\tau + K_3\tau^2 \end{aligned} \tag{3.17}$$

The PID control parametrization in 3.16 is convenient as we can formulate a convex optimization problem for the selection of PID parameters:

$$\min_{K_1,K_2,K_3} \quad \| W_1 \left(GC_{K_1,K_2,K_3} - L \right) \|_\infty \tag{3.18}$$

where W_1 is selected as:

$$\| W_1(j\omega) \| \geq \left| \frac{1}{1 + L(j\omega)} \right|, \ \forall \omega \tag{3.19}$$

This is to preserve the robust stability condition indicated by the small gain theorem:

$$\| S_O \Delta \|_\infty = \left\| \frac{1}{1+L}(GC - L) \right\|_\infty < 1 \tag{3.20}$$

For plant with unstable poles, the target loop selection through H_∞ or LQR design would generally provide better guess in the sense that the stability has more guarantee, while for stable plants, we can simply choose the target loop as $\frac{\lambda}{s}$ if the plant doesn't have any slow poles and choose $\frac{\lambda(s+a)}{s(s+e)}$ if the plant has one or more slow poles. Also as PID controllers has limited degree of freedom, it is required to put a low-pass filter in series with the PID controller to provide enough roll off.

Chapter 4

EXPERIMENT DESIGN AND IMPLEMENTATION OF CONTROLLERS

4.1 Introduction

In this chapter, VTOL drone we conducted the system identification on in this project is shown and a brief introduction to the system identification experiment procedures is made. The implementation of the controllers is discussed, including the hardware and software libraries used in the project and some details of converting PID parameters to a real controller.

4.2 Description of the VTOL Drone

The three-view drawing of the VTOL is shown in Figure 4. Figure 5 provides a 3D graph of the VTOL drone and. Figure 6 provides a photo of the drone in hovering state. The VTOL drone has two symmetric ailerons (longer) and two symmetric rudders (shorter). The wing configuration is similar to the Lockheed XFV-1. The lift force for taking off is generated from the contra-rotating propellers. For the convenience of achieving horizontal flying in the future, the Euler angle directions are defined as shown in Figure 4. When the drone is placed on the ground in rest, the Euler angles with respect to the drone body and with respect to the ground are regarded as overlapping.

As in the vicinity of zero, the Euler angles are decoupled, the yaw and pitch dynamics can be treated as decoupled systems. We can control the yaw and pitch

angles through rudders and ailerons separately when the plane is in the hovering state.

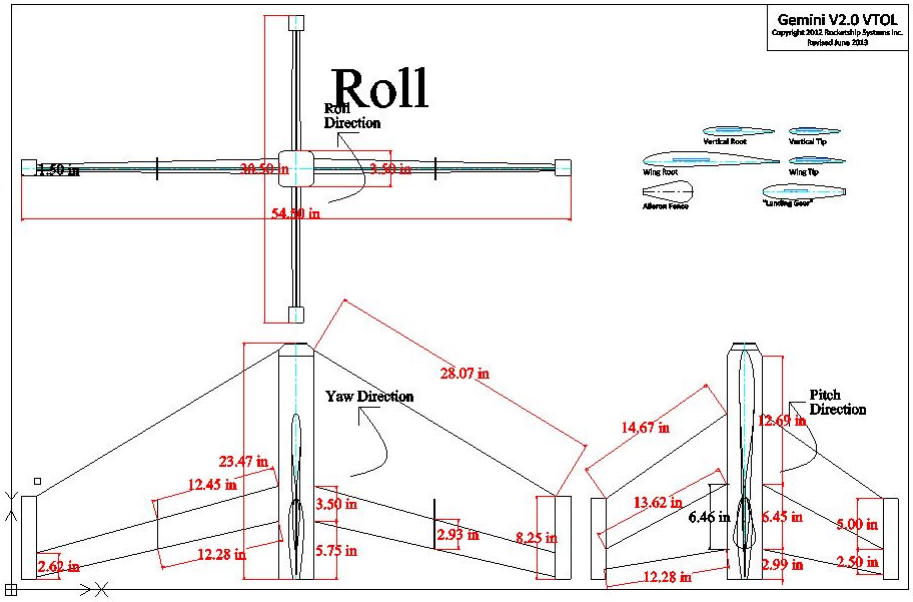

Figure 4. Three-view drawing of the VTOL drone we studied in this project

4.3 System Identification Experiments

In this project, we conducted three system identification experiments. The first one is the open-loop identification, the second one is an intermediate closed-loop identification and the third one is the closed-loop identification. In the first and third experiments, we recorded the reference signals that were fed into the servos that control the flaps on rudders and ailerons as inputs to the system, and we recorded the yaw and pitch angular rates and Euler angles as system output. It should be noted that in the recorded data sets, the reference signals we recorded are subtracted by

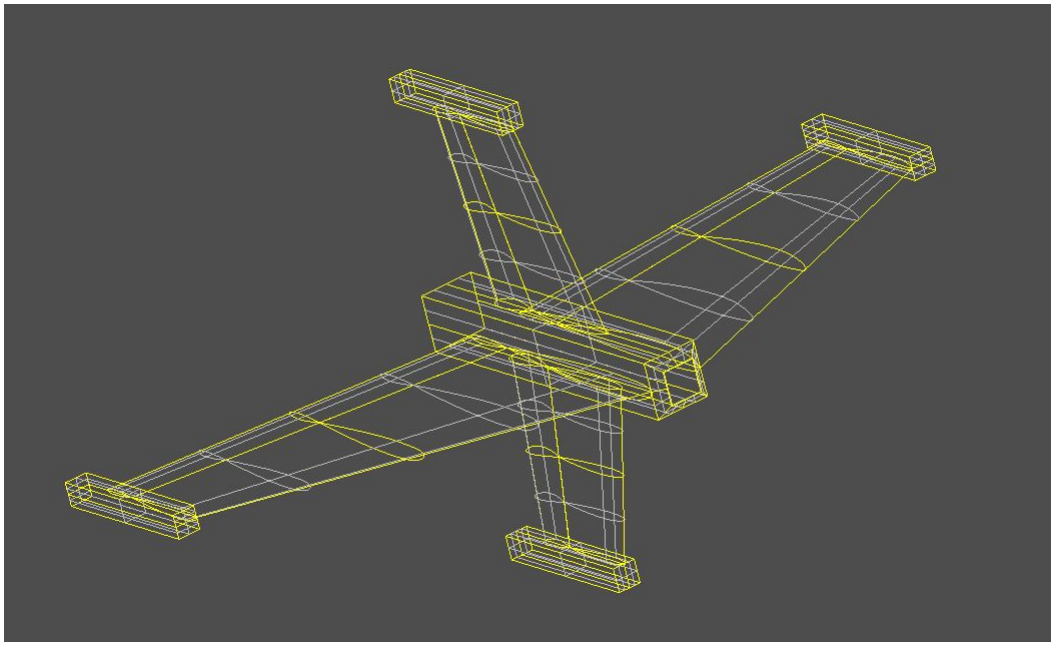

Figure 5. 3D Graph of the VTOL drone we studied in this project

Figure 6. A picture of the VTOL drone we studied in this project in hovering state

1490μs which is the reference for the neutral position of rudders and ailerons. In the intermediate closed-loop identification, we record the difference of the speed references that were fed to the two electronic speed controllers (and eventually to the two motors that provide lift to the drone) as input and the roll angular velocity as output.

In open-loop identification, we used 4 tethers each with one end connected to the drone and the other end connected to a ring that was set on a rod penetrated to the ground to constrain the movement of the VTOL drone. The PRBS (pseudo random binary sequence) signals were added to the reference signals. Afterward we truncated the data recorded in this process and selected those segments where the VTOL drone was not hitting the theaters for system identification.

In the intermediate closed-loop experiment, VTOL drone movement wasn't constrained by any physical connections, and the yaw and pitch actions of the VTOL drone was regulated by controllers designed for the system identification result in open-loop stage. PRBS signals were injected at the output of the controller. At this step, the drone could stay longer in the air and longer data set is recorded.

In the closed-loop experiment, we used the same setup as the intermediate closed-loop experiment where the drone is not contained by tethers. In this experiment, as all three rotations were regulated, longer data sets were acquired.

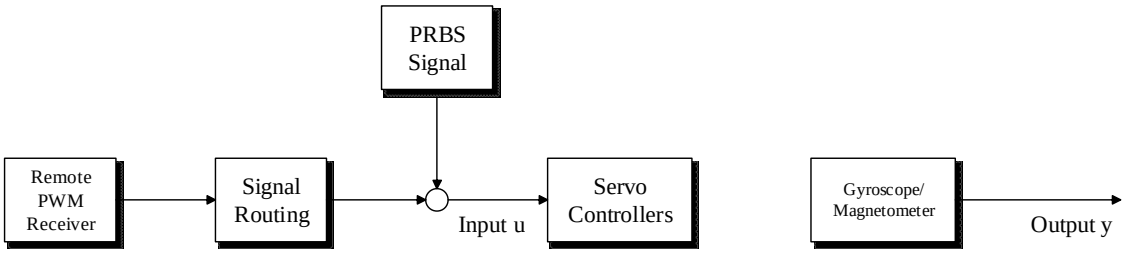

Figure 7. Diagram of the control program used in the open-loop experiment.

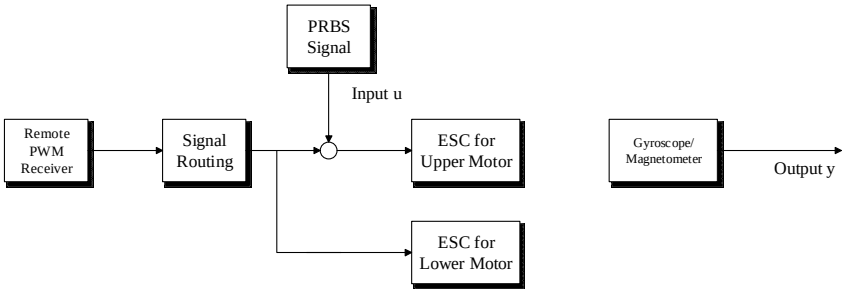

Figure 8. Diagram of the control program used in the intermediate closed-loop experiment.

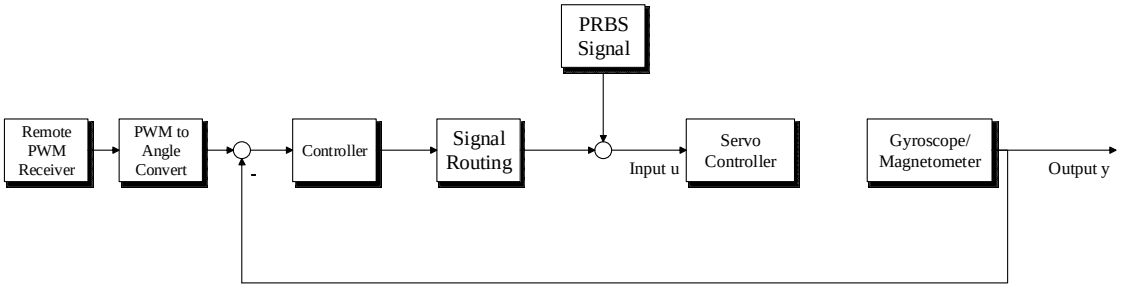

Figure 9. Diagram of the control program used in the closed-loop experiment.

4.4 Hardware and Software Libraries

For the PRBS signals design, we used the method from [2]. The bandwidth of the PRBS was designed to be higher than the bandwidth of the system to guarantee sufficient excitation as described in [9] by Fairweather *et al.* The PRBS generator has a 6 bit shift register and the minimum switching time is 0.05 sec. Thus a single full length of the PRBS signal is 3.15 sec.

In this project, we used Arduino DUE for building controller, reading sensor signal, reading PWM receiver output, and sending measurements/input signals. Arduino Mini Pro was used for recording input and output signals to an SD card. For the sensor, we used GY-86 integrated gyroscope/accelerometer/magnetometer/barometer break board.

FreeIMU open source library was used for reading signals from GY-86 board and the fusion functions in it were used for getting clean measurements. We also made use of the model based design feature from MATLAB Simulink for creating control programs that run on Arduino DUE.

4.5 Implementation of PID Controller Design

PID controllers are straightforward for implementation for their simple structures. Basically a PID controller comprises of a gain element K_p, an integrator $\frac{K_i}{s}$, and a differentiator $K_d s$.

The first issue with a PID controller is that a differentiator couldn't exist in continuous system. The solution to this is replacing $K_d s$ with a low pass filter $K_d \frac{s}{\tau s+1}$ which has a small time constant τ to mimic a differentiator. The time constant τ is usually selected as $\omega_c/100$ where ω_c is the targeted cross over frequency of the loop $G(s)C(s)$.

The second issue is the wind-up phenomenon. As all actuators have saturation limits, once the output of the controller (input to the actuator) hits this limit, the plant output would keep deviating from the reference signal while the integrator keeps integrating the error signal. And this will lead to the failure of control. The solution to this issue is setting a saturation limit which is smaller than the saturation limit of the actuator on the integrator and hold the integrator output as long as the output is staying at the limit. It is also critical to eliminate the bias in the sensor output as it will accelerate the saturation of the integrator. In some cases, a dead-zone should be conservatively considered.

The third issue is the initialization. In some filtering algorithms, the measurement will take time to get to zero. For example, in this project the Euler angle measure-

ment will take 30-40s to be zero depending on the parameters selected for sensor fusion algorithm. In this case, the integrator should be disabled during the sensor initialization process to avoid the integral action that will lead to saturation before the drone taking off. It is also critical to eliminate the bias in the sensor output as it will accelerate the saturation of the integrator.

Chapter 5

EXPERIMENT RESULTS

5.1 Introduction

In this chapter, the results from all three identification experiments with procedure introduced in Chapter 4 are presented. Also included is the controller design based on the results from identification experiments.

This chapter begins by reviewing the identification results from open-loop experiment, including transfer function, singular values, estimation errors and uncertainties identified in the system. Next, controller designed for the system identified is shown including the parameters and step response features. The same thing is conducted on both the intermediate closed loop experiment and closed loop experiment data.

Next, the robust stability condition is being checked through comparing the complementary sensitivity and sensitivity to the corresponding uncertainties.

Last, the verification of controller design is presented by showing the reference tracking performance of the regulated system.

5.2 Open-Loop System Identification Experiment Results

The input and output data we collected from the open-loop experiment was shown in Figure 10, it comprises of 5 discontinuous data sets and the sample rate is 100Hz. However as the measurement contains high frequency noise (e.g. vibration of the motor), it is necessary to carry out a pre-filtering on the collected data to add weights to the frequency domain so that the information contained in the frequen-

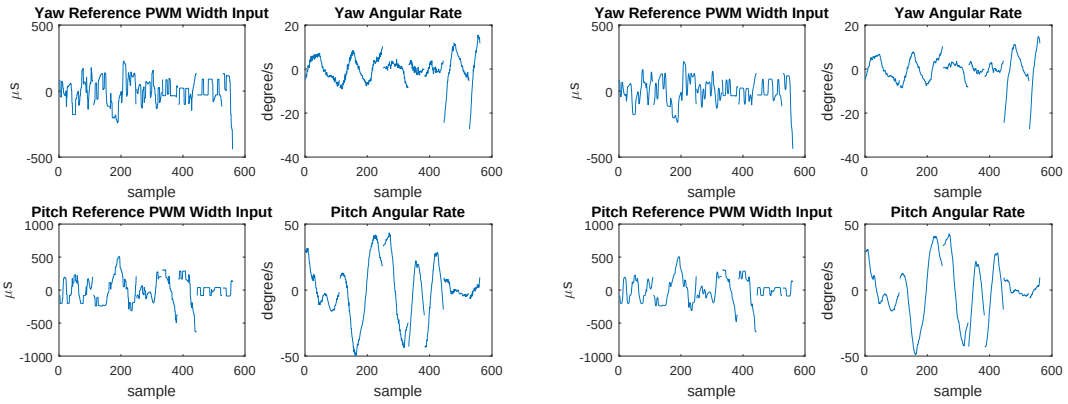

(a) Raw (b) Filtered

Figure 10. NaN-separated data sets collected from open-loop system identification experiment.

cies around bandwidth will be emphasized. The pre-filter we used was a digital filter $\frac{0.7127z+0.1299}{z^2-0.1642z+0.006738}$ with sample rate 100Hz and bandwidth 162 rad/s. For the equivalency of the transfer functions, both the input and output should be filtered with the pre-filter.

Then the algorithms described in Chapter 2 was used for the identification, the pole for the auxiliary filter was -5rad/s. The singular value of the system was shown in Figure 11 and the Bode magnitude plot was shown in Figure 12.

For the purpose of providing constraints for controller design, the multiplicative and divisive uncertainties were computed and shown in Figure 13.

The DC gain of the system transfer function matrix is $\begin{bmatrix} 5.62 \times 10^{-1} & 1.61 \times 10^{-1} \\ -1.57 \times 10^{-2} & 8.28 \times 10^{-1} \end{bmatrix}$, we can approximate treat the system as a diagonal system that the yaw direction and pitch direction are decoupled. Having this approximation, it is possible to design controllers for the diagonal elements of the transfer function matrix only.

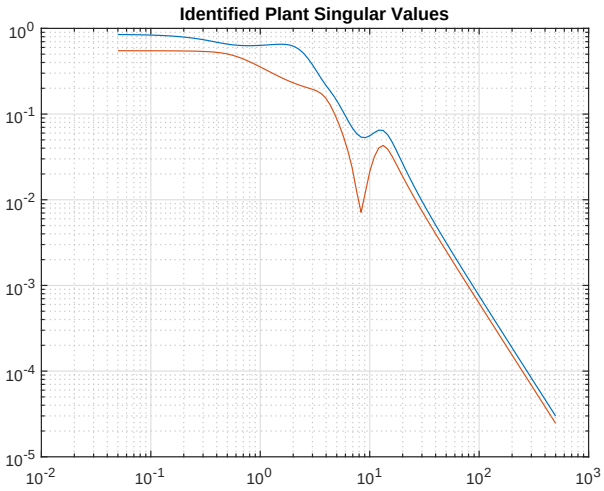

Figure 11. Singular value of the system identified from the open-loop experiment data sets

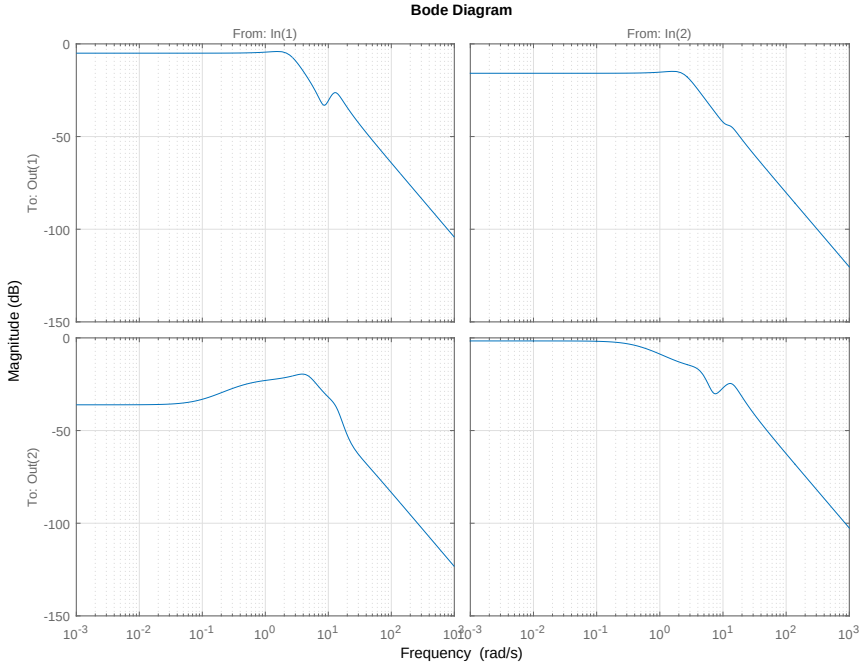

Figure 12. Bode magnitude plot of the system identified from the open-loop experiment data sets

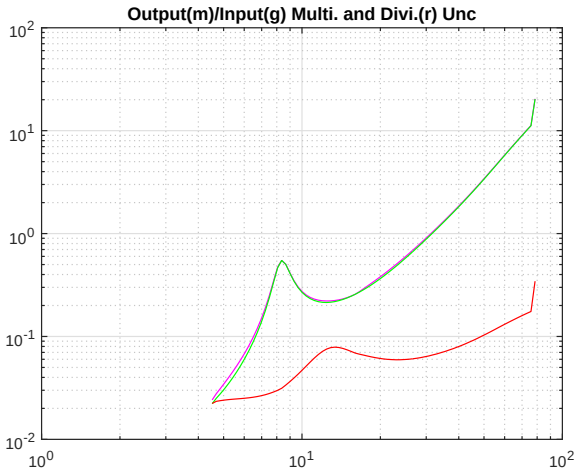

Figure 13. Multiplicative uncertainties and divisive uncertainties computed from the open-loop experiment data sets

By using the methods in Chapter 4, second order low pass filters were used provide PID controllers with higher degree of freedom. The controller selected is $\frac{10}{s+10}$ and it was converted to a digital filter $\frac{0.04762z+0.04762}{z-0.9048}$ by Tustin method for Simulink implementation. The PID controllers along with the low pass filters for the yaw and pitch direction angular rate are

$$\begin{aligned} C_{YawRate}(s) &= \left(4.04 + 3.71\frac{1}{s} + 0.532\frac{s}{0.01s+1}\right)\frac{10}{s+10} \\ C_{PitchRate}(s) &= \left(19.8 + 15.5\frac{1}{s} + 0.505\frac{s}{0.01s+1}\right)\frac{10}{s+10} \end{aligned} \tag{5.1}$$

The above controllers regulates the angular rate, however, we still need controller to regulate the angles. Thus we augmented the complementary sensitivity function $T_{Rate}(s)$of the angular rate control feedback loops with integrators $1/s$ and designed controllers for the new systems $\frac{T_{Rate}(s)}{s}$ that regulates the yaw and pitch angles at the vicinity of 0 which are:

$$\begin{aligned} C_{YawAngle}(s) &= \left(1.04 + 0.312\frac{1}{s} + 0.0542\frac{s}{0.01s+1}\right) \\ C_{PitchAngle}(s) &= \left(1.49 + 1.15\frac{1}{s} + 0.0654\frac{s}{0.01s+1}\right) \end{aligned} \tag{5.2}$$

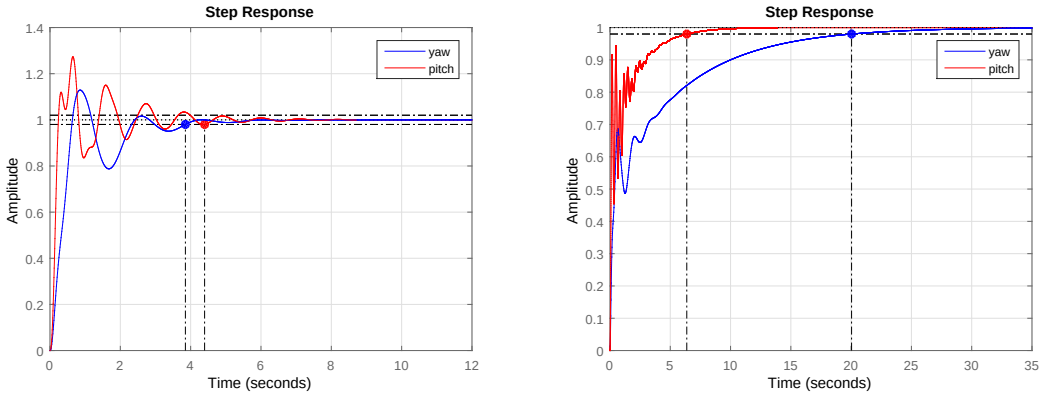

(a) Inner Loop (Angular Rate) Control (b) Outer Loop (Angle) Control

Figure 14. Step responses of inner and outer loops with controllers designed for the system identified from the open-loop system identification experiment.

And the step responses of the inner and outer loops are as shown in Figure 14.

In Figure 14, there are oscillations in the response due to the fact that PID structured controllers have only 3 degrees (4 to 5 if augmented by a low-pass filter) of freedom and the loop shaping result may have some approximation error if the system to be controlled has high orders. However, this is a preliminary result and better results will be acquired in the following experiments.

5.3 Intermediate Closed-Loop System Identification Results

With the above controllers, we stabilized the pitch and yaw actions and made sure that the drone would not fall in the hovering state. In order to make the drone more easy for users to control, we need to stabilize the roll actions. The drone is lifted up by a pair of contra-rotators, and the difference in the torques of the two motors would generate a torque that would make the drone rotate in the vertical direction.

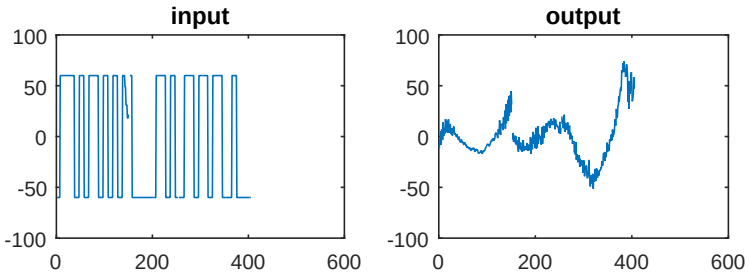

Figure 15. Data sets for roll action system identification.

We had an intermediate closed-loop test to identification the transfer function from the difference in the torque to the roll angular velocity.

We had a total of three data sets from the experiment and they were shown in Figure 15. The data sets have a clear structure, and we didn't used any frequency weightings in the identification. By using the method introduced in Chapter 2 and some iterations on the order and bandwidth of the target, we came to a 3rd order system with 2 zeros. The singular value of the system is shown in Figure 16, and the estimated uncertainties are shown in Figure 17. With the identified system ready, we could now proceed to the controller design. By using the loop-shaping method introduced in Chapter 3, the PID controller we designed to regulate the roll action is:

$$C_{RollRate}(s) = \left(2.67 + 20\frac{1}{s} + 1.66\frac{s}{0.01s+1}\right) \tag{5.3}$$

And the step response of the loop is shown in Figure 18.

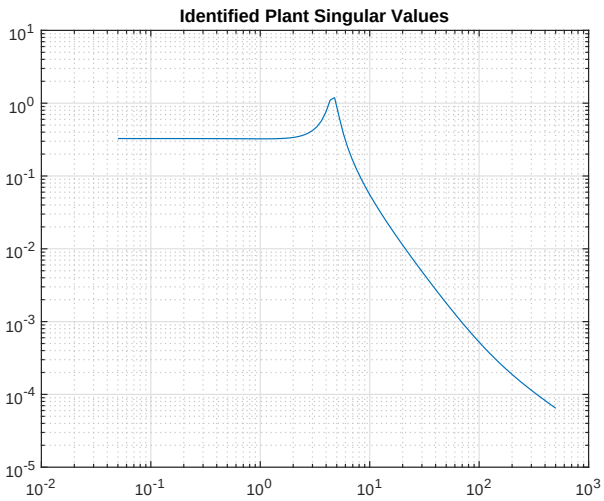

Figure 16. Singular value of the identified system that describes the roll dynamics.

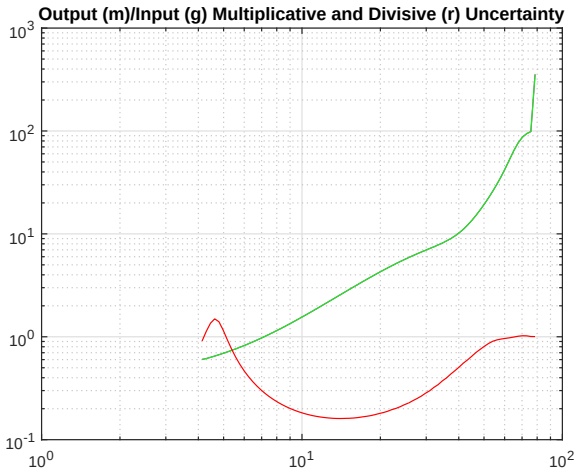

Figure 17. Estimated Uncertainties in the identified system for roll angular velocity dynamics.

5.4 Closed-Loop System Identification Experiment Results

In this section, we used one single data set for system identification and 5 discontinuous data sets for uncertainty computation. The data set for system identification is shown in Figure 19 and the data sets for uncertainty computation are as shown in

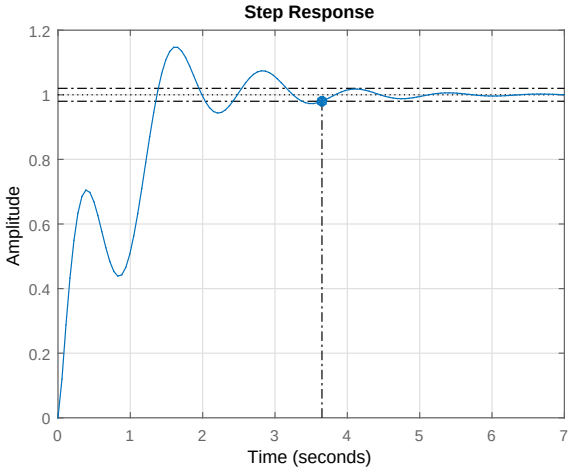

Figure 18. Step response of the controlled roll dynamics.

Figure 20. In this stage, we used the raw data for uncertainty computation while a pre-filtered data set was used for system identification. The pre-filter was a Chebyshev II filter with order of 4, the stop-band attenuation was 45dB and the stop-band edge frequency was 20Hz.

By using the algorithms introduced in Chapter 2, a new system is identified. The pole of the auxiliary filter was -60rad/s which is below the Nyquist frequency. The singular values of the new system is as shown in Figure 21, and the bode magnitude plots are as shown in Figure 22. Next the multiplicative and divisive uncertainties were computed and they are shown in Figure 23.

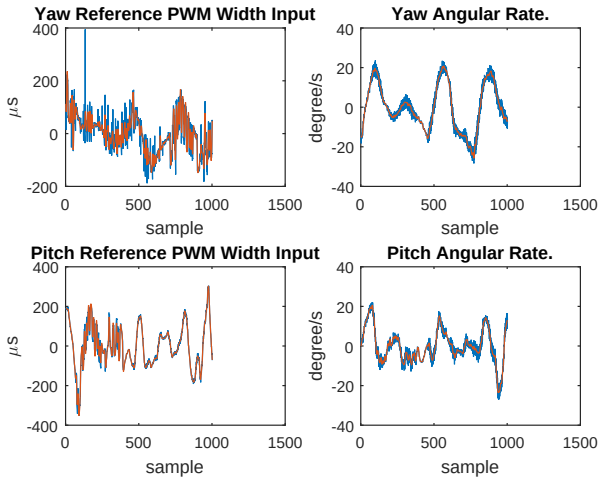

Figure 19. Raw and filtered data sets from the closed-loop system identification experiment for the computation of the system. Blue: raw data; Red: filtered data.

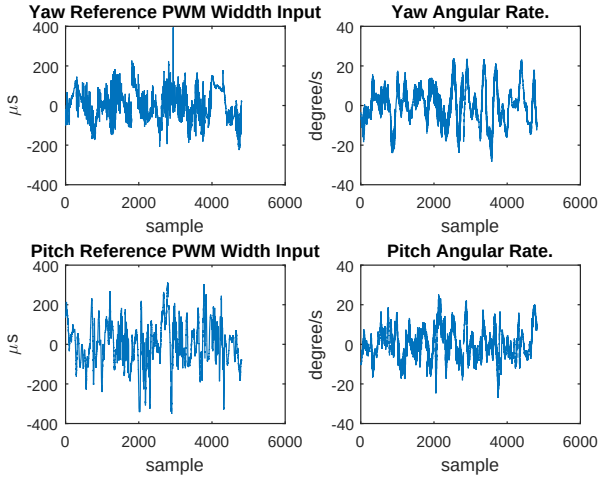

Figure 20. Nan-seperated discontinuous raw data sets from the closed-loop system identification experiment.

The DC gain of the system transfer function matrix is $\begin{bmatrix} 3.3441 & 0.33095 \\ -0.47298 & 2.5984 \end{bmatrix}$, we can still approximate treat the system as a diagonal system that the yaw direction and pitch direction are decoupled as the case in section 5.1. We also adopted the two-loop control where an inner controller regulates the angular rate and an outer

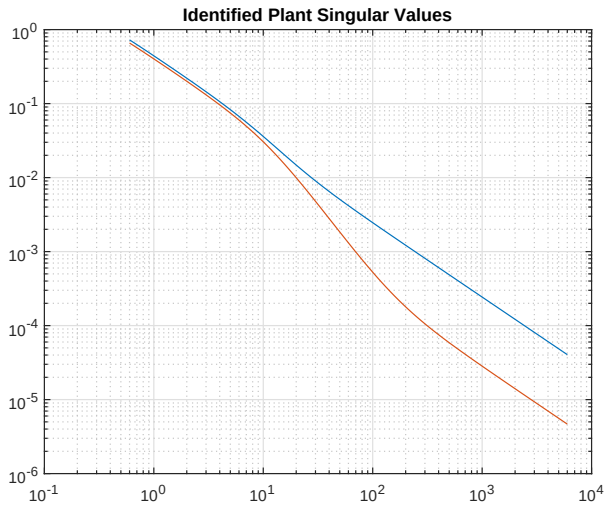

Figure 21. Singular values for the system identified from the closed-loop experiment data

controller regulates the angle. Both inner and outer controllers are PID structures augmented by low-pass filters as before:

$$
\begin{aligned}
C_{YawRate}(s) &= \left(0.405 + 1.24\frac{1}{s} + 0.0309\frac{s}{0.01s+1}\right)\left(\frac{1+s/0.13}{(1+s/8)^2}\right) \\
C_{PitchRate}(s) &= \left(10.3 + 15.5\frac{1}{s} - 0.103\frac{s}{0.01s+1}\right)\left(\frac{1+s/0.16}{(1+s/8)^2}\right) \\
C_{YawAngle}(s) &= \left(1.98 + 0.961\frac{1}{s} + 0.0904\frac{s}{0.01s+1}\right) \\
C_{PitchAngle}(s) &= \left(2.05 + 1.03\frac{1}{s} + 0.0709\frac{s}{0.01s+1}\right)
\end{aligned}
\tag{5.4}
$$

The step response of the inner and outer loop are shown in Figure 24.

5.5 Robust Stability Condition Verification

Robust stability conditions (RSC) stated by equation 2.26 and equation 2.31 are checked by comparing the complementary sensitivity functions or sensitivity func-

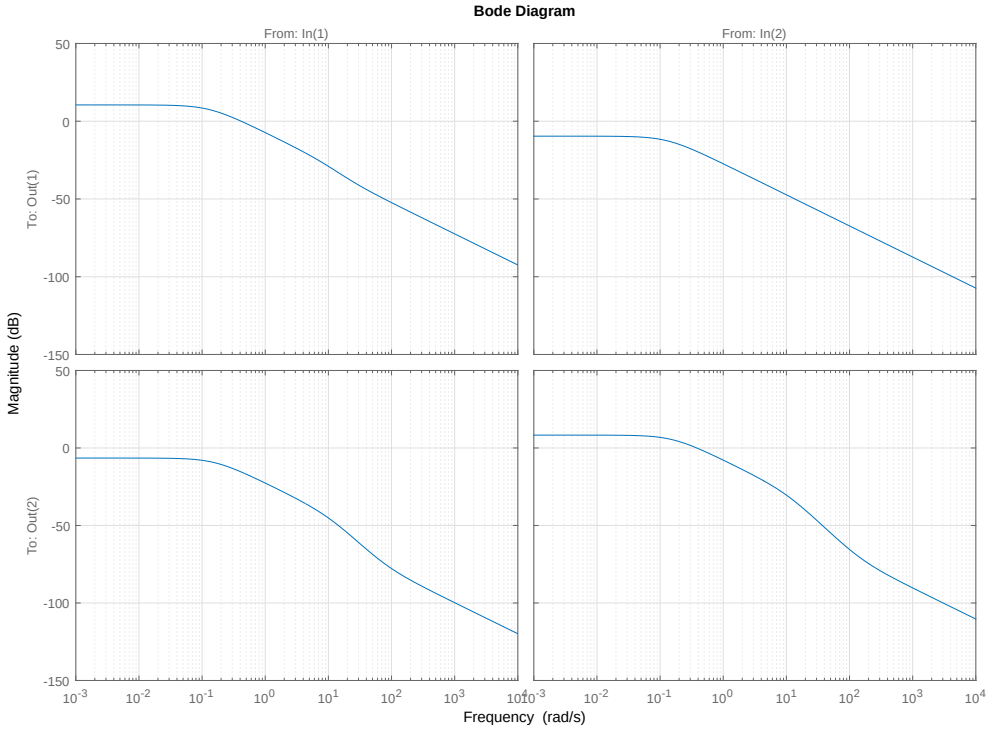

Figure 22. Bode magnitude plots for the system identified from the closed-loop experiment data

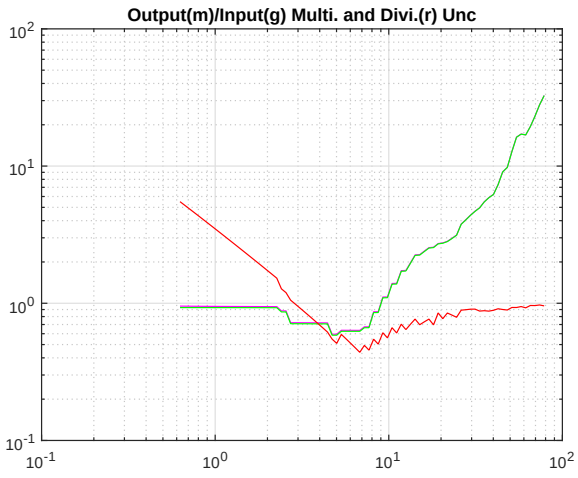

Figure 23. Multiplicative and divisive uncertainties of the system identified from the closed-loop experiment data.

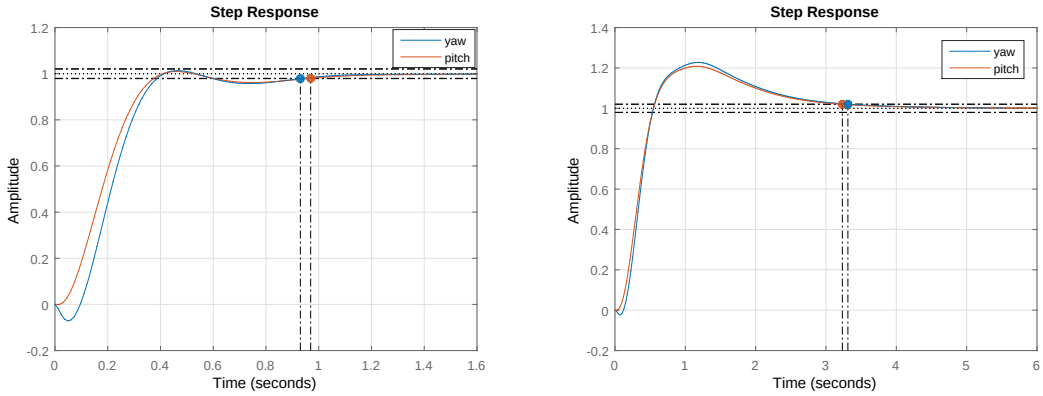

(a) Inner Loop (Angular Rate) Control (b) Outer Loop (Angle) Control

Figure 24. Step responses of inner and outer loops with controllers designed for the system identified from the closed-loop system identification experiment.

tions with their bounds indicated by uncertainties. Here the RSC expressed in 2.31 was adopted.

For the inner loop (yaw and angular rates) controllers for the systems identified from the open-loop and the closed-loop experiments, the RSC is verified in Figure 25. For the controller regulating the roll direction dynamics identified in the intermediate closed-loop experiment, the RSC is verified in Figure 26.

It should be noticed that for the controllers designed for the system identified from the open-loop experiment data, we still need to test the RSC for the outer loop separately. The RSC for the inner loop could be verified directly by checking 2.31, however, for the two loop structure shown in Figure 27, the RSC should be modified to be in form of 5.5 which only considers the SISO case, however similar results could be derived for the MIMO case.

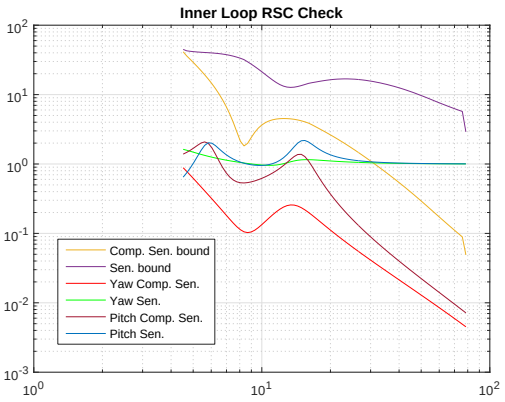

(a) System identified from the open-loop experiment

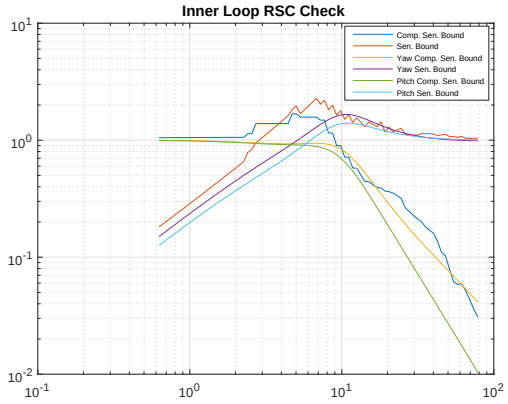

(b) System identified from the open-loop experiment

Figure 25. RSC verification for inner loop (yaw and pitch angular rates) controllers

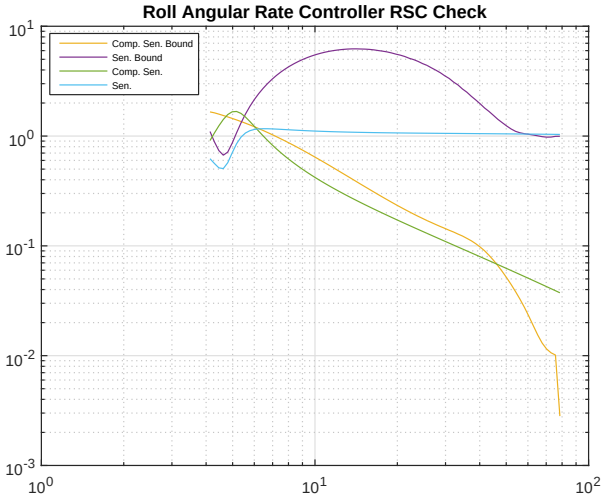

Figure 26. RSC verification for the intermediate closed-loop result roll rate regulation.

$$\begin{aligned} \left\| \left(\frac{(1+C_oP_o)C_iP_i}{1+C_iP_i+C_oP_o+C_iP_iC_oP_o} \right) \Delta T_i \right\|_\infty &< 1 \\ \left\| \left(\frac{1}{1+C_iP_i+C_oP_o+C_iP_iC_oP_o} \right) \Delta S_i \right\|_\infty &< 1 \end{aligned} \tag{5.5}$$

Since the Euler angles were recorded in the closed loop experiment, we can run a system identification from the Euler angle rates to Euler angles to confirm that

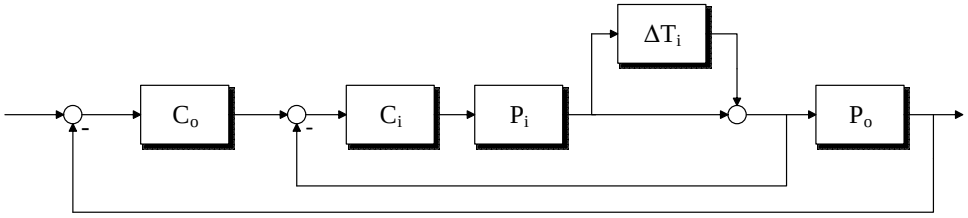

Figure 27. Two loop structure with multiplicative uncertainty for inner loop plant.

the system P_o in Figure 27 is an integrator. The singular values of the system P_o is shown in Figure 28 and the uncertainties are shown in Figure 29. The data sets used for identifying the system is shown in Figure 30 and the data sets used for computing the uncertainties are shown in Figure 31. In the singular values plot, the system is shown to a -20dB/Dec roll off rate, which is exactly what integrators should look like. And the uncertainties shown in Figure 29 is small which implies that the integrator is an good approximation of P_o.

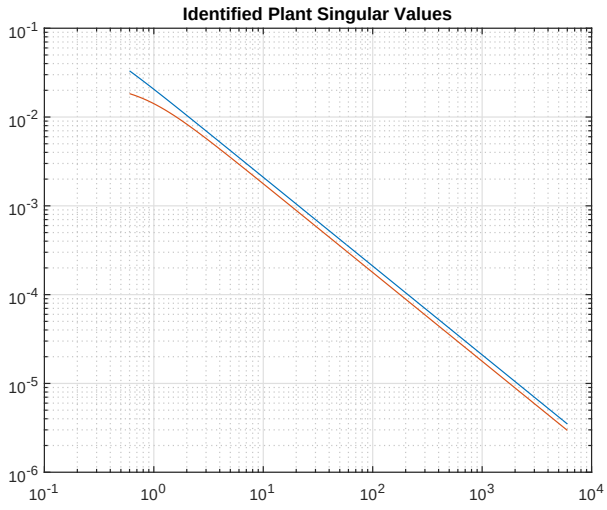

Figure 28. Singular value of the system identified from the data set in which the input is the yaw and pitch angular rates and the output is the yaw and pitch angles.

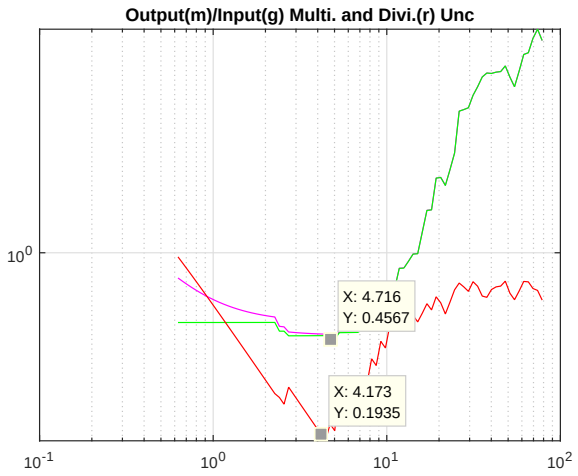

Figure 29. Uncertainties of P_o.

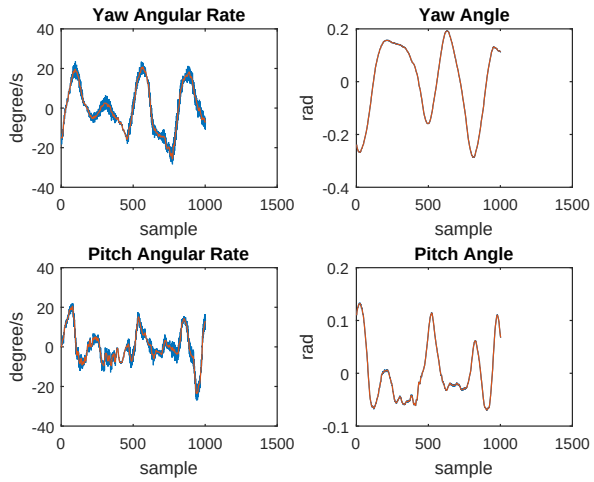

Figure 30. Data set used for the integral relation verification. Blue: raw data; Red: filtered data

The RSC's of the outer loop (yaw and angles) controllers for the systems identified from the open-loop and the closed-loop experiments is verified in Figure 32.

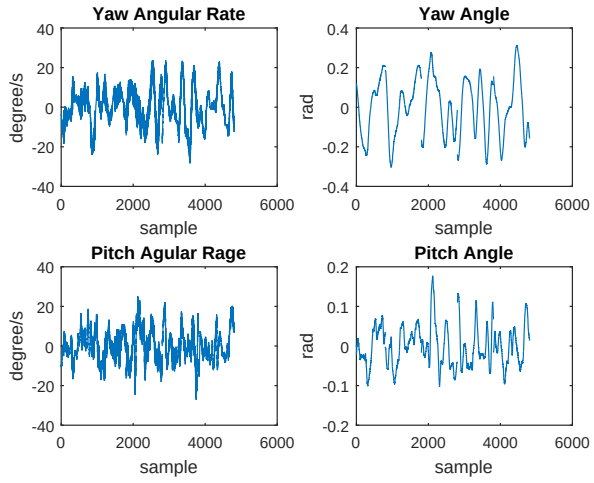

Figure 31. NaN-separated Data sets used for uncertainties computation of P_o.

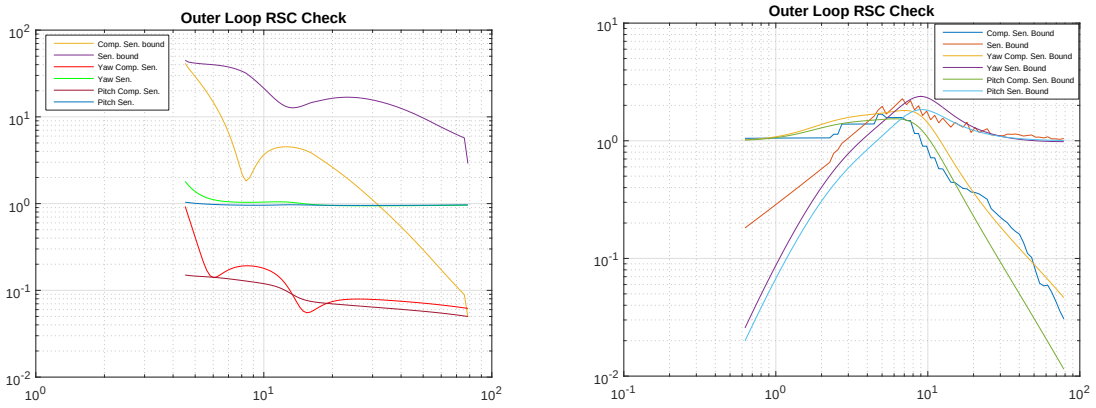

(a) System identified from the open-loop experiment

(b) System identified from the open-loop experiment

Figure 32. RSC verification for outer loop (yaw and pitch angles) controllers

5.6 Reference Tracking Performance in Closed-loop Experiment

In this section we show the reference following performance of the controllers designed for both the model identified from the open-loop experiment and the model identified from the closed-loop experiment. In Figure 34, we show results of two experiments where the reference tracking performances of the yaw and pitch con-

trollers designed for yaw and pitch dynamics identified from the open-loop experiment data sets were tested. In the test, the operator will give yaw/pitch angle commands to the drone through the remoter. The yaw/pitch angle commands are within the range of $-10°$ to $10°$. In the figure, yaw control is not so well. And there is bias in the pitch angle output of the system, due to the poor low frequency accuracy the data sets for identification can provide.

In Figure 33, we show two experiments where the reference tracking performance of the roll controller designed for roll dynamics identified from the intermediate closed-loop experiment was tested. In the test, the reference given by the operator stays at 0 for most of the time. As this is a preliminary result, the reference tracking is not so well, and the controller can barely maintain the roll angular rate staying at zero.

In Figure 35, results of two experiments that test the reference tracking performances of the yaw and pitch controllers designed for yaw and pitch dynamics identified from the closed-loop experiment data sets were shown. The operator did the same thing as in the first test. The performance is greatly improved as the controllers are faster and the model is more accurate.

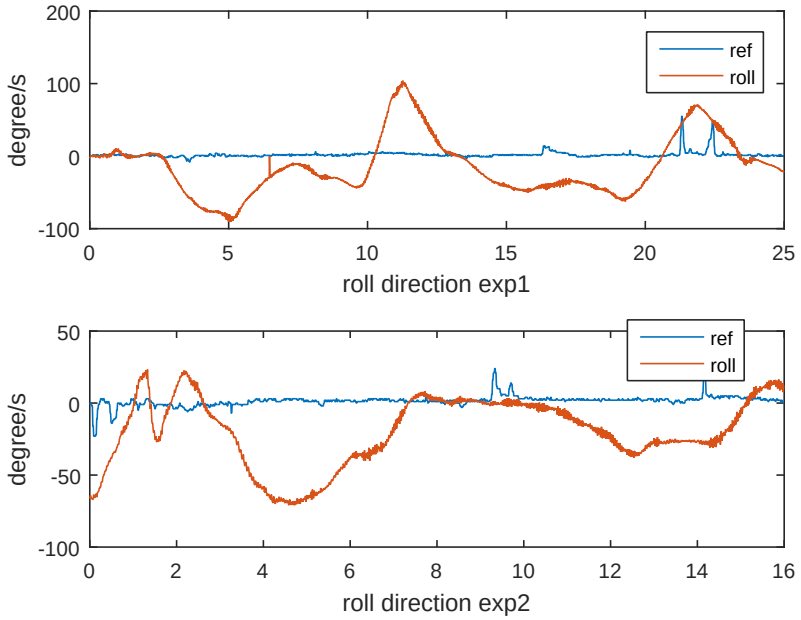

Figure 33. Reference tracking performance of the roll control system from the intermediate closed-loop experiment.

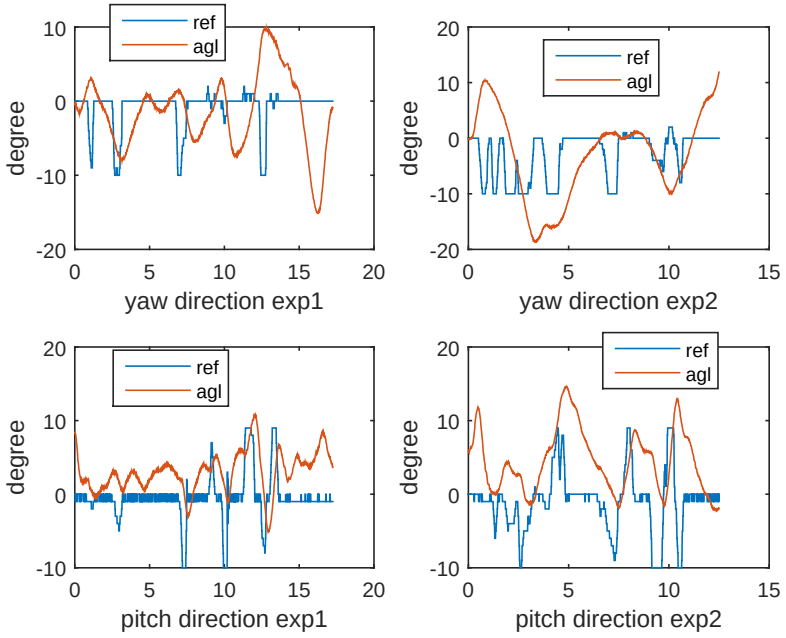

Figure 34. Reference tracking performance of the yaw and pitch control system from the open-loop experiment.

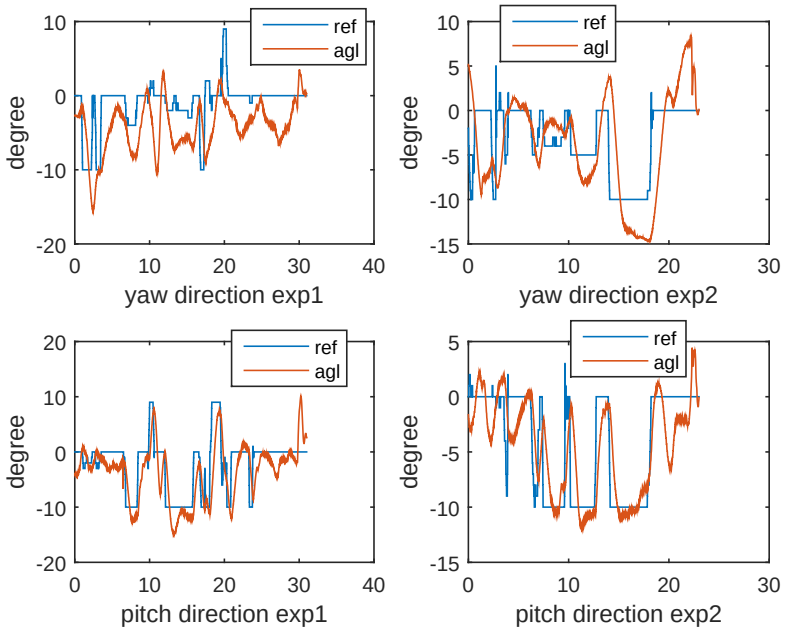

Figure 35. Reference tracking performance of the yaw and pitch control system from the closed-loop experiment.

Chapter 6

CONCLUSION AND FUTURE WORK

6.1 Conclusion of Current Work

This project is to develop an alternative method of building models and designing controllers for VTOL drones. Our current work enables the drone to stay hovering and respond to reference signals that command it to tilt with small angles and thus move horizontally.

The system identification way of building models helps us circumvent the aerodynamics and refine the model by iterating on system identification experiments. As indicated by the well-known saying all models are wrong but some are useful by G.E.P Box in [4], this method of building models ensures the system dynamics of interest are captured instead of building nonlinear models that takes all corner-cases into consideration which would compromise the straightforwardness of analyzing.

The method of identifying models from discontinuous data sets is a powerful tool as input-output data sets that are recorded with non-zero initial state could be used to refine the identification. Also characterizing the estimation error into uncertainties gives alleviation to the conflict between fitting into model and fitting into noise. And this alleviation is augmented when combined with certain level of pre-filtering.

Controller design with the restriction of robust stability condition gives confidence in the controller and enables the controller work while the system deviates from the linearization point with certain degree. Sometimes bounds that are unrealistic for controller design could be resulted from low SNR in the measured output, especially when raw data are used for uncertainty computation while filtered data

sets are used for system identification. In this case, iterations on the assumption of system structure is necessary for a successful identification. However using raw data for uncertainty computation gives more confidence while less flexibility for controller design and using filtered data for uncertainty computation leads to conservativeness.

Last but not least, the experiment could be iterated as controllers with better performance could be designed from data sets collected in experiments. And with longer single data sets collected, the low-frequency performance of the identification could be improved indicating less bias in the system parameters.

6.2 Future Work

The to-do list of this project would be considerable long. However several high-priority improvements should be implemented first. The first is to use H_∞ or LQR controllers directly instead of loop-shaping them into PID controllers augmented by low-pass filters. This would give more better guarantee for the robust stability conditions.

The second thing would be to get longer single data sets so as to acquire more reliable models for control design. Also we should explore the implementation of various adaptive control algorithms to regulate the drone even it is deviated from the hovering state.

The ultimate goal of this project is to achieve switching between vertical hovering and horizontal flying. This would need more delicate design of identification experiments. Also a nonlinear description of the system would be necessary to fully capture the dynamics.

REFERENCES

[1] Adusumilli, S., S. Dash, D. Rivera and K. Tsakalis, "A comparison of identification-based performance bounds for robust process control", in "Control Applications, 1999. Proceedings of the 1999 IEEE International Conference on", vol. 1, pp. 594–599 (IEEE, 1999).

[2] Amrani, M., R. Dowdeswell, P. Payne and K. Persaud, "Pseudo-random binary sequence interrogation technique for gas sensors", Sensors and Actuators B: Chemical **47**, 1, 118–124 (1998).

[3] Bouabdallah, S., P. Murrieri and R. Siegwart, "Design and control of an indoor micro quadrotor", in "Robotics and Automation, 2004. Proceedings. ICRA'04. 2004 IEEE International Conference on", vol. 5, pp. 4393–4398 (IEEE, 2004).

[4] Box, G. E., "All models are wrong, but some are useful", Launer, RL (1979).

[5] Caron, F., E. Duflos, D. Pomorski and P. Vanheeghe, "Gps/imu data fusion using multisensor kalman filtering: introduction of contextual aspects", Information Fusion **7**, 2, 221–230 (2006).

[6] Ding, F. and H. Duan, "Two-stage parameter estimation algorithms for box–jenkins systems", IET Signal Processing **7**, 8, 646–654 (2013).

[7] Ding, F., X. P. Liu and G. Liu, "Identification methods for hammerstein nonlinear systems", Digital Signal Processing **21**, 2, 215–238 (2011).

[8] Ding, J., C. Fan and J. Lin, "Auxiliary model based parameter estimation for dual-rate output error systems with colored noise", Applied Mathematical Modelling **37**, 6, 4051–4058 (2013).

[9] Fairweather, A., M. Foster and D. Stone, "Battery parameter identification with pseudo random binary sequence excitation (prbs)", Journal of Power Sources **196**, 22, 9398–9406 (2011).

[10] Georgiou, T. T., "On the computation of the gap metric", Systems & Control Letters **11**, 4, 253–257 (1988).

[11] Gevers, M. *et al.*, "System identification without lennart ljung: what would have been different?", Forever Ljung in System Identification, Studentlitteratur AB, Norrtalje (2006).

[12] Grassi, E. and K. Tsakalis, "Pid controller tuning by frequency loop-shaping", in "Decision and Control, 1996., Proceedings of the 35th IEEE Conference on", vol. 4, pp. 4776–4781 (IEEE, 1996).

[13] Grassi, E. and K. Tsakalis, "Pid controller tuning by frequency loop-shaping: application to diffusion furnace temperature control", Control Systems Technology, IEEE Transactions on **8**, 5, 842–847 (2000).

[14] Jensen, K. J., "Generalized nonlinear complementary attitude filter", Journal of Guidance, Control, and Dynamics **34**, 5, 1588–1593 (2011).

[15] Kothare, M. V., V. Balakrishnan and M. Morari, "Robust constrained model predictive control using linear matrix inequalities", Automatica **32**, 10, 1361–1379 (1996).

[16] Legarra, A. and V. Ducrocq, "Computational strategies for national integration of phenotypic, genomic, and pedigree data in a single-step best linear unbiased prediction", Journal of dairy Science **95**, 8, 4629–4645 (2012).

[17] Ljung, L., "System identification: Theory for the user", PTR Prentice Hall Information and System Sciences Series **198** (1987).

[18] Ljung, L., "Prediction error estimation methods", Circuits, Systems and Signal Processing **21**, 1, 11–21 (2002).

[19] Madgwick, S. O., "An efficient orientation filter for inertial and inertial/magnetic sensor arrays", Report x-io and University of Bristol (UK) (2010).

[20] Madgwick, S. O., A. J. Harrison and R. Vaidyanathan, "Estimation of imu and marg orientation using a gradient descent algorithm", in "Rehabilitation Robotics (ICORR), 2011 IEEE International Conference on", pp. 1–7 (IEEE, 2011).

[21] Mahony, R., T. Hamel and J.-M. Pflimlin, "Nonlinear complementary filters on the special orthogonal group", Automatic Control, IEEE Transactions on **53**, 5, 1203–1218 (2008).

[22] Mau, S., "What is the kalman filter and how can it be used for data fusión?", Robotics Math pp. 16–811 (2005).

[23] McFarlane, D. and K. Glover, "A loop-shaping design procedure using h∞ synthesis", Automatic Control, IEEE Transactions on **37**, 6, 759–769 (1992).

[24] McRuer, D. T., D. Graham and I. Ashkenas, *Aircraft dynamics and automatic control* (Princeton University Press, 2014).

[25] Naidu, D. S., *Optimal control systems* (CRC press, 2002).

[26] Qin, S. J., "An overview of subspace identification", Computers & chemical engineering **30**, 10, 1502–1513 (2006).

[27] Saavedra-Montes, A., J. Ramirez-Scarpetta, C. Ramos-Paja and O. Malik, "Identification of excitation systems with the generator online", Electric Power Systems Research **87**, 1–9 (2012).

[28] Shafique, A. B. and K. Tsakalis, "Discrete-time pid controller tuning using frequency loop-shaping", in "Advances in PID Control", vol. 2, pp. 613–618 (2012).

[29] Sjöberg, J., Q. Zhang, L. Ljung, A. Benveniste, B. Delyon, P.-Y. Glorennec, H. Hjalmarsson and A. Juditsky, "Nonlinear black-box modeling in system identification: a unified overview", Automatica **31**, 12, 1691–1724 (1995).

[30] Stoorvogel, A. A., *The H_∞ Control Problem: A State Space Approach* (Prentice Hall., 1992).

[31] Tsakalis, K., S. Dash, A. Green and W. MacArthur, "Loop-shaping controller design from input-output data: application to a paper machine simulator", Control Systems Technology, IEEE Transactions on **10**, 1, 127–136 (2002).

[32] Tsakalis, K. and P. Ioannou, "Linear time varying systems: Control and adaptationprentice-hall", Englewood Cliffs, NJ (1993).

[33] Tsakalis, K. and K. Stoddard, "Integrated identification and control for diffusion/cvd furnaces", in "Emerging Technologies and Factory Automation Proceedings, 1997. ETFA'97., 1997 6th International Conference on", pp. 514–519 (IEEE, 1997).

[34] Tsakalis, K. and K. Stoddard, "Control oriented uncertainty estimation in system identification", in "17th IASTED Int. Conf. MIC, Grindelwald, Switzerland", (1998).

[35] Van den Hof, P. M., R. J. Schrama, R. A. de Callafon and O. H. Bosgra, "Identification of normalised coprime plant factors from closed-loop experimental data", European Journal of Control **1**, 1, 62–74 (1995).

[36] Van Overschee, P. and B. De Moor, *Subspace identification for linear systems: Theory—Implementation—Applications* (Springer Science & Business Media, 2012).

[37] Varesano, F., "Prototyping orientation and motion sensing objects with open hardware", in "Proceedings of the 7th International Conference on Tangible, Embedded and Embodied Interaction", pp. 415–418 (ACM, 2013).

[38] Varesano, F. and F. Vernero, "Introducing palla, a novel input device for leisure activities: a case study on a tangible video game for seniors", in "Proceedings of the 4th International Conference on Fun and Games", pp. 35–44 (ACM, 2012).

[39] Wang, D., L. Kaplan, H. Le and T. Abdelzaher, "On truth discovery in social sensing: A maximum likelihood estimation approach", in "Proceedings of the 11th international conference on Information Processing in Sensor Networks", pp. 233–244 (ACM, 2012).

[40] Welch, P. D., "The use of fast fourier transform for the estimation of power spectra: A method based on time averaging over short, modified periodograms", IEEE Transactions on audio and electroacoustics **15**, 2, 70–73 (1967).

[41] Zhan, C. Q. and K. Tsakalis, "System identification for robust control", in "American Control Conference, 2007. ACC'07", pp. 846–851 (IEEE, 2007).

[42] Zhan, C. Q. and K. Tsakalis, "A new robust-control-oriented system identification method", in "Proceedings of the 17th World Congress, The International Federation of Automatic Control", pp. 6–11 (2008).

[43] Zhou, K., J. C. Doyle, K. Glover *et al.*, *Robust and optimal control*, vol. 40 (Prentice hall New Jersey, 1996).